AD-A162 415 CHARACTERIZATION OF THE GENERAL ELECTRIC CID-17 AS A DETECTOR FOR PLASMA (U) ARIZONA UNIV TUCSON DEPT OF CHEMISTRY R B BILHORN ET AL 25 NOV 85 TR-42 1/1

UNCLASSIFIED N00014-83-K-0268 F/G 20/9 NL

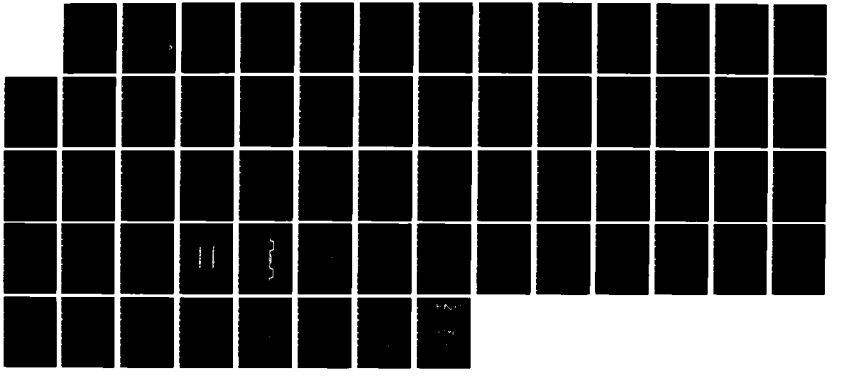

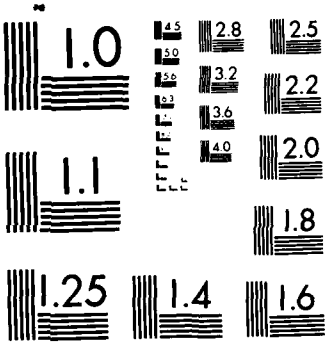

SECURITY CLASSIFICATION OF THIS PAGE (When Data Entered)

REPORT DOCUMENTATION PAGE

READ INSTRUCTIONS BEFORE COMPLETING FORM

1. REPORT NUMBER: 42	2. GOVT ACCESSION NO.
3. RECIPIENT'S CATALOG NUMBER	
4. TITLE (and Subtitle): Characterization of the General Electric CID-17 as a Detector for Plasma Emission Spectrometry	5. TYPE OF REPORT & PERIOD COVERED: Interim
	6. PERFORMING ORG. REPORT NUMBER
7. AUTHOR(s): Robert B. Bilhorn and M. B. Denton	8. CONTRACT OR GRANT NUMBER(s): N00014-83-K-0263
9. PERFORMING ORGANIZATION NAME AND ADDRESS: Department of Chemistry, University of Arizona, Tucson, Arizona 35721	10. PROGRAM ELEMENT, PROJECT, TASK AREA & WORK UNIT NUMBERS: NR 051-549
11. CONTROLLING OFFICE NAME AND ADDRESS: Office of Naval Research, Arlington, Virginia 22217	12. REPORT DATE: November 25, 1985 13. NUMBER OF PAGES: 57
14. MONITORING AGENCY NAME & ADDRESS(if different from Controlling Office)	15. SECURITY CLASS. (of this report): unclassified 15a. DECLASSIFICATION/ DOWNGRADING SCHEDULE

16. DISTRIBUTION STATEMENT (of this Report)

17. DISTRIBUTION STATEMENT (of the abstract entered in Block 20, if different from Report)

18. SUPPLEMENTARY NOTES

Prepared for publication in Applied Spectroscopy

19. KEY WORDS (Continue on reverse side if necessary and identify by block number)

Charge Injection Device (CID)

20. ABSTRACT (Continue on reverse side if necessary and identify by block number)

Rapid qualitative and quantitative elemental analysis of complex mixtures by optical emission spectrometry requires sensitive simultaneous multiwavelength detection. Until the present, this has been possible only by employing a number of discrete detectors. All types of detectors for plasma emission spectroscopy must meet a series of demanding requirements. Among these are high quantum yield over a wide wavelength range, low noise and a very wide dynamic range. The need for a multichannel detector which meets these requirements has long been recognized but only now satisfied. (Continued on other side.)

DD FORM 1 JAN 73 1473 EDITION OF 1 NOV 65 IS OBSOLETE

S/N 0102-LF-014-6601

SECURITY CLASSIFICATION OF THIS PAGE (When Data Entered)

Studies in this laboratory employing a General Electric Co. CID-11B have indicated that the Charge Injection Device possesses characteristics which make it an ideal detector for atomic spectroscopy. The newer CID-17, having more detector elements and a device geometry which would suggest an enhanced ultraviolet response, was a logical choice for continued research in this area. An array camera system based on this device has been designed, constructed and evaluated in this laboratory. It has been found to meet all of the requirements for use as a detector for plasma emission spectrometry and over some wavelength ranges to be far superior to photomultiplier tubes. With almost 100,000 channels, true multiwavelength detection is obtained making a new wealth of information available to the analytical chemist.

OFFICE OF NAVAL RESEARCH

Contract N00014-83-K-0268

Task No. NR 051-549

TECHNICAL REPORT NO. 42

Characterization of the General Electric CID-17 as a Detector For Plasma Emission Spectrometry

by

Robert B. Bilhorn and M. Bonner Denton

Prepared for Publication in

Applied Spectroscopy

Department of Chemistry
University of Arizona
Tucson, Arizona 85721

November 25, 1985

ABSTRACT

Rapid qualitative and quantitative elemental analysis of complex mixtures by optical emission spectrometry requires sensitive simultaneous multiwavelength detection. Until the present, this has been possible only by employing a number of discrete detectors. All types of detectors for plasma emission spectroscopy must meet a series of demanding requirements. Among these are high quantum yield over a wide wavelength range, low noise and a very wide dynamic range. The need for a multichannel detector which meets these requirements has long been recognized but only now satisfied.

Studies in this laboratory employing a General Electric Co. CID-11B have indicated that this device possesses characteristics which make it an ideal detector for atomic spectroscopy. The newer CID-17, having more detector elements and a device geometry which would suggest an enhanced ultraviolet response, was a logical choice for continued research in this area. An array camera system based on this device has been designed, constructed and evaluated in this laboratory. It has been found to meet all of the requirements for use as a detector for plasma emission spectrometry and to be far superior to photomultiplier tubes over some wavelength ranges. With 96,000 channels, true multiwavelength detection is obtained making a new wealth of information available to the analytical chemist.

INTRODUCTION

The benefits of simultaneous multielement analysis, simultaneous background correction and rapid qualitative analysis have prompted many investigations into the application of TV type multichannel detectors to atomic absorption, atomic fluorescence and atomic emission spectroscopy (1-8). The more recent attempts have involved the use of silicon vidicons and photodiode arrays (PDAs) in various intensified and unintensified configurations to replace the photomultiplier tubes and or photographic film found at the focal plane of conventional scanning and direct reading spectrometers. These approaches have met with some success, however, advantages in simultaneity are accompanied by losses in sensitivity and other difficulties such as insufficient dynamic range in the case of vidicons, and insufficient number of resolution elements in the case of photodiode arrays. The problems are particularly severe in the case of atomic emission spectroscopy (AES) where spectral line intensities can vary over five or more orders of magnitude and where high resolution coverage of a wide wavelength range is necessary.

The charge injection device (CID) offers several unique characteristics which help it overcome the problems of sensitivity and dynamic range which have plagued the application of imaging detectors to AES. Additionally, the CID offers very good geometric accuracy and freedom from distortion inherent in digitally addressed solid state devices, as well as a very large number of resolution elements. A new generation CID, the General Electric Co. CID-17 (9) will be shown to have more detector elements, lower crosstalk and enhanced UV response as compared to the CID-11B evaluated earlier in these

laboratories (10). Before a description of the properties of the CID-17, the spectroscopically pertinent characteristics of other commercially available imaging detectors will be reviewed so that direct comparisons can be made.

Difficulties with vidicons such as their fragile nature, hysteresis and blooming have resulted in extensive efforts on the part of television camera manufacturers to seek solid-state replacements. These difficulties are much the same as those that limit the applicability of vidicons to spectroscopic analysis. The spectroscopically pertinent characteristics of vidicons have been extensively studied with regard to their application in UV/VIS absorbtion spectrometry and AES (11-13). Poor sensitivity, low dynamic range, blooming, high dark current at room temperature or lag at low temperature, high read noise, and poor image fidelity (pincushion distortion) are among the shortcomings that limit the usefulness of these detectors in analytical spectroscopy.

Photodiode arrays have been investigated as alternatives to vidicons for multiwavelength detection in AES as they have been found to overcome many of the problems associated with vidicons (14-18). Photodiode arrays offer very high geometric accuracy, no read lag and are much less susceptible to blooming. Linear photodiode arrays (LPDA) manufactured for scientific applications (such as the Reticon Corporation S series linear photodiode arrays) have high aspect ratio sensing sites or detector elements (100:1) designed to couple well to the exit slits of conventional spectrometers. The large area of these detector elements (2.5 mm x 25 μm = 0.0625 mm^2) with respect to other commercially available arrays allows a large photogenerated charge storage capacity or full well capacity (8 X 10^7 charge carriers). A theoretical dynamic range can be

calculated by dividing the full well capacity by the system read noise. In the case of these large detector element arrays, a relatively large theoretical dynamic range is calculated. In practice, this large theoretical dynamic range is not realized because of limitations imposed by the 14-bit analog-to-digital converters which are commonly employed and because of significant dark current build up rates. These limitations are not fundamental, however. Dark current can be eliminated in the LPDA as well as in other solid state detectors by cooling below the -20 C, which is common. Approximately a factor of 2 reduction in dark current is seen for every 8 K drop in temperature.

LPDAs are available with up to 2048 detector elements from Reticon Corporation. Coverage of the entire visible and ultraviolet portions of the spectrum at adequate resolution for AES (≈0.01 nm) is not possible with an array having so few detector elements, so wavelength coverage must be sacrificed when using a LPDA by observing only small portions of the UV/VIS spectrum at a time. This is conventionally done by sequentially monitoring small contiguous segments of the spectrum (4,8,18). A more efficient and elegant approach is to monitor several specially chosen noncontiguous segments (19).

A principal drawback of PDAs is the very high noise levels associated with reading out a detector element as compared to certain other solid-state devices developed to replace tube type imagers. Such imagers include charge coupled devices (CCDs) and CIDs. The noise associated with reading out a single detector element is termed read noise and is usually reported as a rms value in terms of equivalent photogenerated electrons. Several sources contribute to the total read noise in an imager, each adding in quadrature. Thorough discussions of these various

noise sources and their relative magnitudes have been published (16,20-23), hence only a brief discussion of the most important sources will be presented here. The high read noise observed in PDAs is due in part to the high video output capacitance which results from the video line being connected to the drain junction of the multiplex switch associated with each diode (Figure 1). This high video output capacitance results in a high equivalent input noise at the preamplifier as shown in Equation 1.

$$N_{J,PDA} = \frac{C_v}{q} \left(4kT\Delta f \frac{k_0}{g_m}\right)^{\frac{1}{2}} \qquad (1)$$

where C_v = video line capacitance,

q = electron charge,

k = Boltzmann's constant,

T = operating temperature,

Δf = bandwidth (Hz), and

k_0/g_m = channel resistance of the input transistor.

The direct proportionality between video line capacitance and preamplifier noise results in this noise contribution being significant in Reticon S series linear photodiode arrays which can have video line capacitances up to 24 pf (≥4). Another important noise source in photodiode arrays is KTC noise, also known as thermodynamic noise or switch noise. This noise results from the uncertainty in voltage

level left on a diode capacitance after opening the reset switch. The magnitude of this uncertainty is given by Equation 2.

$$N_{KTC} = 1/q\ [kT(2C_d + 2C_c)]^{\frac{1}{2}} \qquad (2)$$

where C_d = diode capacitance and

C_c = clock line to video line capacitance.

The factor of 2 in the above equation is introduced because as one diode is connected to the video line, another is disconnected (22). Diode capacitance of Reticon S series photodiodes is 2 pf (24), which by itself results in a contribution of 738 electrons of noise RMS at -20 C. Although video line capacitance may be reduced by connecting fewer diodes to any one video line, or by other changes in device design, KTC noise is a fundamental noise which is introduced any time a switch is opened and cannot be reduced without reducing switch (diode) capacitance or temperature. Diode capacitance can be reduced by reducing detector element area; however, a sacrifice in dynamic range is also made.

Reported values for total PDA read noise range from 800 electrons for a system employing an array with 0.6 pf diode capacitance (25um X 25um detector elements) built for astronomical use (21), to the noise levels attainable in commercial systems which employ Reticon S series arrays and are on the order of 1500 electrons (17).

Two-dimensional photodiode arrays are available in sizes up to 256 X 256 detector elements (24). These devices would allow the coverage of a much larger spectral region at the required .01 nm resolution for AES if an

echelle grating spectrometer with appropriate image reduction optics were employed (6). Unfortunately, the dynamic range advantage of large detector elements is lost in the two-dimensional array and the video line capacitance is significantly increased. Dynamic range of these devices is on the order of 100 (24,25), and a loss of sensitivity results from the presence of non-photosensitive MOS readout circuits interleaved between the array of photodiodes. The percentage of the array which consists of photoactive sites, known as the optical fill factor, is typically only 25 to 33 percent (25).

Both CCDs and CIDs are capable of attaining much lower read noise levels than photodiode arrays. CCD camera systems are commercially available with read noises on the order of 15 to 50 electrons (20), and laboratory systems have been reported with read noises as low as 10 electrons (27). CID systems have been reported with noise levels as low as 250 electrons (28). These lower noise levels are possible because of fundamental differences in CID and CCD device architecture which avoid high video line capacitance and allow the removal of KTC noise.

The method used for removal of KTC noise in the CID-17 is illustrated in Figure 2 which shows a small section of the sensor. Photogenerated charge is sensed by measuring current or voltage changes on the video line induced by moving charge from the column to row MOS capacitor plates (29,30). Unlike the photodiode array, there are no individual detector element reset switches connected to the video line so the capacitance is low. KTC noise can also be avoided because the row electrode potential can be sampled after resetting it and prior to shifting the charge from the column electrode (28). Unlike the

photodiode, there is no uncertainty in the voltage left on the detector element capacitance after the reset switch is opened.

Optical fill factors of 80 to 100 percent are possible with modern two-dimensional CCDs and CIDs because of the presence of less overlying multiplexing circuitry in the case of CIDs and because of virtual phase fabrication (31,32) or back side illumination (33,34) in CCDs. These higher optical fill factors coupled with lower system read noise result in more sensitive photon detection.

Two-dimensional CCDs and CIDs have full well capacities dictated by detector element area just as photodiode arrays, but because of lower read noise levels, dynamic ranges are larger for CIDs and CCDs than for photodiode arrays with similar detector element dimensions. In spite of this improvement in dynamic range (typically on the order of 1000 to 10,000 charge carriers) these devices do not currently have a sufficiently wide dynamic range to be used for direct imaging in AES.

Methods involving the summation of multiple exposures and using varying integration times for spectral features of varying intensity have been proposed for use with vidicons and PDAs in order to cope with the problem of insufficient dynamic range. These methods are also applicable to CIDs and CCDs. The method of summation of exposures involves summing in computer memory the results of a number of short exposures thus extending the effective saturation level. This method is commonly employed in PDA systems, however, it is undesireable in these read noise limited systems because a read noise component is introduced with every summation. The method of varying integration time proposed for vidicons avoids this problem by allowing weak spectral features to integrate longer than more intense ones. Using this method, read noise is introduced only once

during the measurement process because each spectral feature is interrogated only once after an integration time dependent on its intensity. This method requires prior knowledge of the locations of intense spectral features, however, so that they may be prevented from blooming and destroying the spectral information contained in adjacent detector elements. Prior to an analysis, the locations of all intense spectral features must be mapped and stored in computer memory so that they may be individually accessed. Blooming is prevented by continuing to interrogate the detector elements associated with an intense spectral feature after the measurement of its intensity is made thus eliminating photogenerated charge that would otherwise saturate the detector elements.

The signal-to-noise ratio merits of the varying integration time method are demonstrated in the following example: Assume a charge separation event rate due to photon absorbtion of 10 per second per detector element at the spectral feature of interest, and a total integration time of 200 seconds. Additionally, assume a detector read noise of 1000 carriers and two separate conditions under which measurements will be made. In the first case, the signal will be integrated on the detector for the full 200 seconds. In the second case, some other intense spectral feature will limit the maximum integration time to 20 seconds, requiring 10 successive exposures to be summed in computer memory in order to obtain the desired 200 second observation time. In the first case, the measurement signal-to-noise ratio will be the product of carrier generation rate and integration time divided by the read noise. The resulting SNR is 2. In the second case, the signal will be the same, however, the total noise will be given by the quantity $(10(1000)^2)^{1/2}$, resulting in a signal-to-noise ratio of 0.63. In both cases negligible dark current is assumed as is the case when

solid state detectors are sufficiently cooled. Also, shot noise in the charge separation rate is not considered since it is significantly lower than the assumed read noise. Clearly the on-detector integration method is the more desireable of the two methods.

The on-detector integration method will present significant difficulties when employed with a vidicon system used as a detector for AES. Intense spectral features must be mapped prior to an exposure and the affected areas of the detector read regularly in order to prevent blooming. The varying integration time on-detector method cannot be used with commercially available PDAs or CCDs: in the case of CCDs charge is transferred across the device during the read process, and in the case of linear PDAs, detector elements must be accessed sequentially and hence recharged. A modified version of the multiple exposure method will be possible with new anti-blooming CCDs (TI and RCA 504). In this method a short exposure is made to measure the intensity of strong spectral features and longer exposures will be used to measure the intensity of weak spectral features. Manufacturers claim that blooming is controlled in these devices up to 10,000 times saturation, so intense spectral features should not hamper the measurement of the intensity of the weak spectral features.

A unique read mode of the CID, the nondestructive read mode (35-38), enables extension of the dynamic range of this device by using the varying integration time method without imposing the "prior knowledge" limitation. As the name suggests, the photogenerated charge information contained at a detector element can be measured without destroying the information. Thus, detector elements can be interrogated during exposure and those nearing saturation read destructively to prevent blooming. This method of extending dynamic range has been effectively

demonstrated using the General Electric Co. CID-11B sensor as a detector for AES (10).

The ability to mix destructive and nondestructive reads distinguishes the CID from all other array detectors and makes it uniquely suitable for AES for two reasons. The first is that individual detector elements may be interrogated as to how much photogenerated charge has accumulated while photons are still being collected and without disturbing the charge information already stored. Based on the signal level measured, a decision can be made to either continue integrating photons or to read the signal level, store the integration time and then discontinue monitoring that particular site. This removes the "prior knowledge" limitation imposed on the vidicon or other detectors which do not allow a nondestructive read. The second reason is that the nondestructive read allows reduction of the system read noise and hence enhancement of the signal-to-noise ratio. The sources of system read noise in the CID include the first stage of the video preamplifier and several on-chip sources. These include Johnson noise due to the resistance of the row bus and the channel resistance of the row select switches. A major component of the read noise is white or random, and so by reading the same charge information multiple times and averaging, the contribution of this component can be reduced.

The low read noise levels attainable with CIDs and CCDs put them in direct competition with photomultiplier tubes (PMT) used in the "photon counting" mode for low light level detection. Relatively low photocathode quantum efficiencies and finite photocathode dark current limit the signal-to- noise performance of photomultiplier tubes at low light levels. The signal-to-noise ratio in the PMT cathode photocurrent, in the absence of dark current, is the SNR in the incident photon beam degraded by the

less than unity quantum efficiency of the photocathode. The signal-to-noise ratio expressed in electrons for an incident photon flux of ϕ_p observed for a time interval t is:

$$S/N_{p,rms} = (n\phi_p t)^{\frac{1}{2}} \qquad (3)$$

where n = photocathode quantum efficiency. The principal noise source in the photon-counting PMT is shot noise in the photocathode dark current (39). This shot noise, in electrons, is given by:

$$N_s = (\phi_e t)^{\frac{1}{2}} \qquad (4)$$

where ϕ_e = the flux of thermal electrons. The signal-to-noise ratio measured at the anode is then given by;

$$S/N_{pmt,rms} = [(n\phi_p + \phi_e)t]^{\frac{1}{2}} \qquad (5)$$

In contrast to the PMT (40), monolithic silicon imagers can be cooled sufficiently to eliminate dark current. Thus, the only significant noise source in these devices is the noise associated with reading the charge information at a detector element site. The expected signal-to-noise ratio for one of these devices is given by Equation 6.

$$S/N_{ctd,rms} = (n\phi_p t + N_r^2)^{\frac{1}{2}} \qquad (6)$$

where N_r = the rms system read noise in charge carriers.

The consequence of this is that at low light levels the S/N attained with the solid state imager should improve more rapidly with integration time than the S/N attained with the PMT. Eventually, the S/N attained with the solid state imager is expected to surpass the S/N attained with the PMT. The point in time at which the solid state imager will yield a higher S/N ratio depends on the photon flux, the quantum efficiency of the two detectors at the wavelength of the incident photons, the photocathode dark current and the imager read noise.

The assumption is made that the photon flux is integrated on a single detector element. This is not an unfair bias against PMTs since a photomultiplier tube placed behind an exit slit only has a small area of its photocathode utilized. Spectrometers have been built to be used with solid state imagers that produce slit images compatible with this assumption (6,10).

Figure 3 shows the calculated S/N performance of a solid state imager versus integration time as compared to the performance of a PMT in photon counting mode for a photon flux of 5 photons per second. The assumptions under which the comparison is made are summarized in the figure. As can also be seen, superior S/N performance will be obtained with the solid state imager at integration times longer than 55 sec. The imager parameters used in the figure were chosen to be consistent with those measured for the imager system described in this manuscript.

EXPERIMENTAL

The General Electric CID-17 sensor is a monolithic silicon imager constructed using metal oxide semiconductor fabrication processes (42). The topology of a four detector element area is illustrated in Figure 4a. Figure 4b shows a cross-sectional view of one detector element. A varying thickness oxide structure is used with two storage capacitors at each detector element site, which is in turn defined by a rectangular thinned oxide region. Two crossed polycrystalline silicon conducting strips form the column and row electrodes as well as the interconnecting buses. The lower conductor forms the column connected capacitor where it crosses the thin oxide and the upper conductor forms a split row capacitor where it crosses the thinned region. The upper polysilicon conductor is thinned and strapped with a narrow metalization in order to enhance transmissivity while maintaining high electrical conductivity. Silicon nitride layers are used with the silicon oxide layers in order to allow thinner insulators to be fabricated and to act as a refractive index matcher to help minimize reflective losses. The relatively simple and transparent structure of these sensors results in high responsivity, and the absence of structures between detector elements results in a high optical fill factor.

Photometrically accurate performance of a CID can only be obtained with custom fabricated drive circuits and amplifiers. The camera system constructed in these laboratories to evaluate the CID-17 is similar to the system described by Sims and Denton for the evaluation of the CID-11B sensor (10). A video preamplifier is housed along with the CID in a liquid nitrogen cryostat (Infrared Laboratories, Tucson, AZ). The video signal

is further amplified and correlated noise removed in a camera head electronics package. The video signal is then digitized to 14 bits and passed to the Model CC183 camera controller (Photometrics Ltd, Tucson, AZ). Table 1 lists the components which make up the host computer system.

Camera data is observed in real time on an X-Y monitor (Hewlett Packard Corporation Model 1332A, Colorado Springs, CO) by sending digital data from the camera to a special monitor driver board along with detector element, line and frame synchronization signals. Digital to analog converters convert the digital intensity data and the output of X and Y axis counters to analog signals which are input to the monitor. High resolution graphics display of processed pictures is accomplished with a 640 column by 480 row scan converter with 256 grey levels and an additional 1 bit graphics plane (Photometrics Ltd. Model 1A, Tucson, AZ 85719) and an Audiotronics model 12VM968 video monitor (North Hollywood, CA).

Tests of device performance were conducted using the test apparatus illustrated in Figure 5. The light source is a red light emitting diode (LED) controlled by the computer through the camera controller. Two small holes (0.25 mm dia) allow the LED to illuminate a small circular region near the center of the detector. The purpose of these aperture stops will be discussed in the description of the crosstalk measurements. The detector is exposed to a controlled amount of light by flashing the LED the desired number of times. The duration of each flash is held constant and only the number of flashes is varied. The effects of junction heating on light output are avoided because the LED is always flashed for the same length of time and long cool down times are allowed between flashes. Typically, duty cycles of less than 1% are used. Experiments are started by flashing the LED a number of times in order to allow the junction

temperature to stabilize. Once the temperature is stable, the exposure level is directly proportional to the number of flashes.

Quantum efficiency measurements as a function of wavelength were made using the test apparatus illustrated in Figure 6. The combination of deuterium and tungsten sources (GCA McPherson Model EU701-50, Acton, MA) provides wavelength coverage from 200 to 1000 nm. A 0.35 meter f 6.8 Czerney-Turner monochromator with a 1080 line/mm grating blazed at 250 nm (GCA McPherson Model EU700, Acton, MA) is used for wavelength dispersion. A 4 inch diameter integrating sphere coated with Eastman white reflectance paint number 6080 ensures even illumination of the detector. A filter holder at the exit slit of the monochromator holds one of a series of interference filters (Balzers, Marlborough, MA) ensuring that second order radiation and stray light are prevented from striking the detector. An electronic shutter (Ilex Optical Co. Model 1, Rochester, NY) controlled by the computer through the camera controller allows exposure of the CID to the source for a precisely known length of time. A photodiode with a calibration traceable to the National Bureau of Standards (EGG Model UV-444BQ) is employed with a picoammeter (Pacific Precision Instruments Model 110, Concord, CA) to measure the photon flux exiting the integrating sphere per square centimeter as a function of wavelength at a precisely known distance from the exit. Calibration of the picoammeter was verified with a reference current source (Heath Model EUA 20-12). Knowing the photon flux from the integrating sphere per square centimeter per second as a function of wavelength and the precise geometry of a detector element, the total number of photons striking a detector element during a given exposure time can be calculated.

RESULTS AND DISCUSSION

Experiments designed to evaluate the effect of multiple nondestructive signal measurements on the signal level actually measured are necessary in order to demonstrate that photometric accuracy can be maintained even when hundreds of re-reads are involved. A truly nondestructive read is necessary in order to employ the varying integration time method discussed above and also to reduce system read noise. The experiments consist of illuminating the array to some arbitrary level using the test apparatus illustrated in Figure 5 and reading a 10 detector element by 10 detector element subarray located near the center of the device nondestructively. The signal level measured at each of the 100 detector elements in the subarray is then averaged. Nondestructive reads of the same charge information are carried out 2000 times and the average signal levels for each read recorded. Ideally, no change in signal level should be observed throughout the process. Typical results of this type of experiment are presented in Figure 7a. Signal level is plotted versus the number of times the subarray was nondestructively read. The figure shows that essentially a constant value is obtained. Figure 7b is the same data plotted on an expanded scale and shows a slight positive trend in signal level. After 2000 reads a signal level shift of about 0.1 percent is observed. The cause of this signal level shift has not been exactly identified, however, it may be the result of a hysteresis effect caused by charged surface states as has been postulated for the CID-11B sensor (43).

Averaging successive nondestructive reads of the charge information stored in a detector element reduces the contribution of white or random noise to the overall system read noise. The degree to which system read

noise can be reduced by this method can be studied by performing increasing numbers of nondestructive reads on the charge information stored in a subarray. The array is illuminated to some arbitrary level using the LED in the test stand and the resulting signal measured in a 10 detector element by 10 detector element subarray. In the case of one nondestructive read, read noise is calculated by reading the signal from the subarray into two 100 element arrays in computer memory. One array is subtracted from the other, point by point, resulting in a difference array having a mean of zero. Because only a single exposure is used, detector element-to-detector element variations due to photon shot noise are subtracted. The deviation of any one element of the difference array from zero is the result of system read noise. The variance in the difference data is then calculated and divided by two to account for the fact that two signal measurements were made for each detector element. Finally, the square root of the value is taken to give the root mean square system read noise.

To measure the reduction in system read noise by performing multiple nondestructive reads, the subarray is read n times and the resulting signal added detector element by detector element to the results of the previous reads in the 100 element array in computer memory. Once all of the n reads are completed, the array is divided point by point by the number of reads performed. The process is then repeated for the second 100 element array before the difference is taken and the variance and rms noise calculated.

The results of this type of experiment are shown in Figure 8. The rms system read noise is plotted on the vertical axis in charge carriers (holes) versus the square root of the number of nondestructive reads

performed. Calculation of read noise in carriers requires knowledge of system gain. The measurement of this parameter will be described. The white noise associated with a system read should be reduced as the square root of the number of times the charge information is sampled. This theoretical behavior is very closely followed. Significant improvements in read noise can be made by continuing the nondestructive read procedure up to 400 times, reducing the system read noise from 960 charge carriers to 60 charge carriers.

The rate at which charge separation events occur due to processes other than the absorbtion of a photon (primarily thermal) is termed dark current. The dark current of the CID-17 camera system was evaluated in a manner similar to the method used to evaluate the effect of re-reads on signal level. The imager was exposed to an arbitrary light level in the test stand and a 10 detector element by 10 detector element subarray read nondestructively. The 100 detector element average was then computed and stored. After waiting for a 20 second time interval, the same 10 by 10 subarray was again read nondestructively, and the average stored. This process was repeated at 20 second intervals for a total of one hour. The average intensity measured at each time interval was then plotted versus the elapsed time, and the slope of the line of best fit taken as the dark current rate. Using this method, the dark current rate was immeasureable within the limits of uncertainty of the experiment (±30 electrons/hour).

The linearity of the response of the detector to light was tested by sequentially exposing the device to higher and higher levels of illumination using the test apparatus and measuring the resulting signal. The linearity experiment is performed by first flashing the array with the red

LED in the test apparatus until the desired incremental increase in illumination level is obtained. The signal is then read nondestructively from a ten detector element by ten detector element subarray and averaged over the 100 detector elements. The array is then exposed to another incremental increase in illumination and, without injecting the previously stored charge, the signal again read out nondestructively. The process is continued, each time the LED flashes adding the same amount of photogenerated charge, and each time the subarray read out nondestructively.

The results of such a linearity experiment are shown in Figure 9a. The signal plotted on the Y axis is in equivalent charge carriers and the light level plotted on the X axis is in the number of times the LED was flashed. The Y intercept is the offset voltage level applied to ensure that no detector elements ever yield a negative signal voltage. The roll off at the upper portion of the curve represents the point of device saturation. The saturation level is ≈500,000 charge carriers. The first derivative of the linearity plot presented in Figure 9b clearly shows a slight negative curvature in the response of the detector to light. This nonlinearity amounts to about 0.2 percent.

If desired, the detector response can be fit quite well to a second order polynomial and the curve linearized to within 0.005 percent. Deviation from linearity is calculated as the rms deviation from the line of best fit. The result of this linearization process is shown graphically in Figures 10a and b which are the linearized counterparts of Figures 9a and b. The time required to perform this linearization is quite short compared to the time required to acquire data in an analysis.

The number of inject cycles required to completely remove all photogenerated charge from the device determines the preparation time

required between exposures. The number of cycles required was measured using the test apparatus and consisted simply of exposing the array to some arbitrary light level, measuring the signal level nondestructively, injecting the array once, measuring the signal level again, and continuing to alternately inject and read the signal level. Ideally all the charge should be removed in as few cycles as possible without exceeding the maximum allowable device operating voltages. Figure 11 shows the results of such a test where signal level is plotted versus the number of inject cycles the device has undergone. The figure shows that a single inject cycle effectively removes all photogenerated charge and that as many as 200 additional inject cycles remove no further charge. The results of this experiment are unaffected by the initial level of photogenerated charge. Injecting the charge from the entire array (96,000 elements) requires ten microseconds.

The evaluation of parameters such as noise level and full well capacity, in terms of charge carriers, as well as the determination of absolute device quantum efficiency, require accurate knowledge of the system gain. This gain is normally expressed in electrons per analog to digital converter unit. The method used for measuring system gain relies on the fact that rms photon shot noise is very nearly equal to the square root of the total photon flux and is called the mean-variance method. Several discussions of the mean-variance method for evaluating gain and read noise of array camera systems have been published (43,44). By using the method of nondestructive reads to reduce the system read noise, the photon shot noise associated with a particular illumination sequence becomes the only dominant noise source. This shot noise can be measured and hence the number of photogenerated charge carriers calculated. Once the number of charge

carriers is known, the system gain is simply calculated by dividing the number of charge carriers by the signal level measured in ADUs.

The gain measurement is made using the test stand. The experiment involves illuminating the array to an arbitrary level and performing a series of nondestructive reads in order to record the photogenerated charge information from a 10 detector element by 10 detector element subarray in a manner relatively free from system read noise. The array is then injected and re-exposed to the LED source for the same time interval. The results of the second exposure are then recorded for the same 10 detector element by 10 detector element subarray using the same number of nondestructive reads as were used for the first exposure. With the system read noise sufficiently reduced, and for sufficiently high exposure levels, detector element to detector element intensity variations between the two exposures will be due to photon shot noise. Subtracting the two arrays one from the other will result in a mean value of zero, and summing the squares of the deviations from zero and dividing by the number of elements will give the variance due to photon shot noise. As in the case of the system noise measurement, this value is divided by two to account for the fact that two exposures were made. The mean value of one of the two signal arrays is calculated prior to the subtraction. This process is then repeated at a variety of different mean signal levels. A plot of variance versus mean signal level has a slope equal to the inverse of the system gain. The slope of the line is not 1 as would be the case if the variance in the number of photons arriving at the detector per unit time were plotted versus mean arrival rate. This is because the system gain factor is included wnen measuring these two quantities. The mean signal level measured is the product of the number of charge carriers produced and the system gain factor. In the case of the

variance calculation, the system gain factor comes in as a square term. In performing the gain measurement, two exposures are made at each exposure level. Any nonreproducibility in illumination level between the two exposures would result in an erroneously high variance measurement. For this reason the means of the two successive signal measurements are adjusted to the same value prior to calculation of the variance due to photon shot noise. This is done by multiplying one of the two arrays point by point by an adjustment factor given by the quotient of the two means. As long as the required adjustment is small, the photon shot noise in each exposure will be unaffected.

The result of the mean-variance measurement used to evaluate the system gain is shown in Figure 12. Each point corresponds to the average of 10 values calculated at that exposure level. Were the system noise low enough, photon shot noise could be observed above system noise and no averaging of nondestructive reads would be required. If this were the case, the y axis intercept would correspond to the system read noise and would provide a convenient method of evaluating this parameter.

The effect of the presence of charge at a detector element site other than the one currently being read on the signal level measured at that detector element site is termed crosstalk. Crosstalk in the CID-17 is very slight but measurable. The crosstalk only occurs along columns, that is, the only stored charge that will have an effect on the signal level measured at a particular detector element is charge stored along the same column as the detector element under consideration. The effect that is observed is an enhancement of the signal measured at a detector element that is proportional to the total amount of charge stored along the column associated with that detector element. The origins of crosstalk

in the CID sensor are described by Sims (43). The observed crosstalk in the CID-17 is less than that observed in the CID-11B described by Sims because of the existence of a row deselect register in the CID-17 (see Figure 13). This row deselect register maintains the potential of all rows not connected to the preamplifier. The absence of this deselect register in the CID-11B allows the potential of the unselected rows to be affected by the charge transfer operation used in the read process. These potential changes can then couple to the active row producing crosstalk (see Figure 14).

The measurement of crosstalk is made using the test apparatus. The two aperture stops allow illumination of the center of the array without exposing the surrounding area to any light. Measurement of signal level at various positions on the array as a function of exposure allows the evaluation of the crosstalk. In areas of the array that are masked from the source, signal level should remain constant at the dark bias level regardless of exposure. If crosstalk occurs, however, the signal level in these dark areas will not remain constant and will depend on the amount of light that has fallen on the rest of the array. In the experiment performed to evaluate the magnitude and functionality of the crosstalk along a column, two subarrays were used. One 20 element array, one detector element wide and 20 detector elements long oriented along a column located entirely within a dark area of the array, was used to test for variation in dark signal level as a function of illumination. This array was chosen to lie within a column that passed through the illuminated region of the CID. The second array consisted of the entire column which contained the first array (see Figure 15). First, bias frames for the two subarrays were stored and then a series of exposures were made using the

LED. Between each exposure, or flash, the first subarray, the one masked from the source, was read and a mean signal level calculated. The mean signal value obtained for this array prior to any illumination was then subtracted and the result reported as crosstalk. The entire column was then read and the sum of the signals from each detector element, less the bias value, was computed. This value was reported as the total column integrated charge. This measurement included the sampling of signal due to crosstalk but because the effect is small, constituted only a small error.

The results of the above experiment are shown in Figure 16. Column crosstalk per detector element in arbitrary converter units is plotted versus the total column integrated charge. The figure shows that crosstalk is directly proportional to total integrated charge and that the magnitude of the effect is on the order of 700 ppm or about 0.07 percent. In the application of atomic emission spectroscopy, crosstalk in the CID-17 is not an important concern and in most cases can be neglected because most of the array is not under intense illumination and hence the total column integrated charge along any one column will never be very large. Because of the very slight crosstalk observed in the CID17, measurements of linearity and gain did not require correction. This resulted in a simplification of these experiments as compared to those used to evaluate the CID-11B. Experiments attempting to measure crosstalk along a row indicated that this type of crosstalk does not occur to a measureable level. This experiment also verifies that the light blocking mask is effective.

The quantum efficiency as a function of wavelength measured for the CID-17 is shown in Figure 17. The quantum efficiency was measured using the apparatus illustrated in Figure 5. For reference, the quantum efficiency curves for several photocathode materials used in photomultiplier tubes are

also plotted. These photocathode materials were chosen because they represent the highest quantum efficiency materials available over the visible and ultraviolet region of the spectrum. None of the photocathode materials listed responds at 1000 nm. It should also be pointed out that the materials that give better quantum efficiency in the red region of the spectrum have much higher dark currents and associated noise levels than the materials that respond in the blue or ultraviolet. Also, semitransparent photocathode materials used in end on photomultiplier tubes have lower quantum efficiencies.

CONCLUSION

The CID-17 precision array camera system constructed and evaluated in these laboratories demonstrates performance superior to all other types of array detectors evaluated to date under the conditions commonly encountered in atomic emission analysis. High quantum efficiency, low read noise, no dark current, minimal crosstalk and more than 95,000 detector elements combine to create a powerful detector system. With no contribution from dark current shot noise, spectral stripping may be performed with only a small degradation in the SNR of the resulting frame. This allows faint spectral features to be observed amidst a complex spectral background. The lack of dark current combined with the ability to intermix destructive and nondestructive reads allows extension of the upper end of device dynamic range. This allows on chip variable integration time detection rather than the summing of multiple exposures in computer memory. The SNR advantages of this approach in conjunction with high device quantum efficiency and low

read noise produce a detector system rivaling PMTs for sensitivity and dynamic range.

ACKNOWLEDGMENT

This research was partially supported by the Office of Naval Research.

REFERENCES

1. D. G. Mitchell, K. W. Jackson and K. M. Aldous, Anal. Chem. 45, 1215A (1973).

2. Micheal J. Milano, Harry L. Pardue, Thomas E. Cook, Robert E. Santini, Dale W. Margerum and John M. T. Raycheba, Anal. Chem. 46, 374 (1974).

3. K. W. Busch, N. G. Howell and G. H. Morrison, Anal. Chem. 46, 2074 (1974).

4. Kenneth M. Aldous, Douglas G. Mitchell and Kenneth W. Jackson, Anal. Chem. 47, 1034 (1975).

5. Thomas E. Cook, Robert E. Santini and Harry L. Pardue, Anal. Chem. 49, 871 (1977).

6. Hugo L. Felkel, Jr. and Harry L. Pardue, Anal. Chem. 49, 1112 (1977).

7. Hugo L. Felkel, Jr. and Harry L. Pardue, Anal. Chem. 50, 602 (1978).

8. Gary Horlick and Edward G. Codding, Anal. Chem. 45, 1490 (1983).

9. D. M. Brown, M. Ghezzi, and M. Garfinkel, IEEE J. Solid State Circuits SC-11, 128 (1976).

10. G. R. Sims and M. B. Denton, "Multielement Emission Spectrometry Using a Charge-Injection Device Detector," in Multichannel Image Detectors, Vol. 2, Yair Talmi, ed., ACS Symposium Series Vol. 236, American Chemical Society, Washington, D.C. (1983), p. 117.

11. John W. Olesik and John P. Walters, "The Silicon-Intensified Target Vidicon Detector: Operation, Characterization, and Application," in Multichannel Image Detectors, Vol. 2, Yair, Talmi, ed., ACS Symposium Series Vol. 236, American Chemical Society, Washington, D.C. (1983), p. 31.

12. Yair Talmi, Anal. Chem. 47, 699A(1975).

13. T. A. Nieman and C. G. Enke, Anal. Chem. 48, 619 (1976).

14. Yair Talmi, Anal. Chem. 47, 658A (1975).

15. Gary Horlick, Appl. Spec. 30, 113 (1976).

16. Yair Talmi and R. W. Simpson, Appl. Opt. 19, 1401 (1980).

17. Yair Talmi and Kenneth W. Busch, "Guidelines for the Selection of Four Optoelectronic Image Detectors," in Multichannel Image Detectors, Vol. 2, Yair Talmi, ed., ACS Symposium Series Vol. 236, American Chemical Society, Washington D.C. (1983), p. 1 .

18. Frederick Grabau and Yair Talmi, "Inductively Coupled Plasma-Atomic Emission Spectroscopy with Multichannel Array Detectors," in Multichannel Image Detectors, Vol. 2, Yair Talmi, ed., ACS Symposium Series Vol 236, American Chemical Society, Washington, D.C. (1983), p. 75.

19. Gilbert M. Levy, Alex Quaglia and Robert Lazure, 1985 Pittsburgh Conference on Chemistry and Spectroscopy, Paper No. 749.

20. Eustace L. Dereniak and Devon G. Crowe, Optical Radiation Detectors, John Wiley and Sons, New York (1984).

21. Steven S. Voight, Robert G. Tull, and Philip Kelton, Appl. Opt. 17, 574 (1978).

22. Raymond W. Simpson, Rev. Sci. Inst. 50, 730 (1979).

23. The Infrared Handbook, William L. Wolfe and George J. Zissis, eds., Office of Naval Research, Department of the Navy, Washington, D.C. (1978).

24. Image Sensing Products, EG&G Reticon, Sunnyvale, CA.

25. G. W. Huges, RCA Engineer 29, 4 (1984).

26. Photometrics Ltd., Tucson, AZ.

27. James R. Janesick, Tom Elliott, Stewart Collins, Harry Marsh, Morley M. Blouke and Jack Freeman, SPIE Proceedings 501, 1 (1984).

28. Richard S. Aikens, AURA Engineering Technical Report No. 66 (1980).

29. Hubert K. Burke and Gerald J. Michon, Proceedings of the IEEE ED-23, 189 (1976).

30. Gerald J. Michon and Hubert K. Burke, 1974 IEEE International Solid-State Circuits Conference Digest of Technical Papers, p. 26.

31. J. Hynecek, Proceedings 1979 IEEE Electron Device Meeting, Washington, D.C. p. 611 (1979).

32. James R. Janesick, J. Hynecek and M. M. Blouke, SPIE Proceedings 290, 165 (1981).

33. R. D. Melen and J. D. Meindl, 1973 IEEE International Solid-State Circuits Conference (New York, 1973) p. 415.

34. S. R. Shortes, W. W. Chan, W. C. Rhines, J. B. Barton and D. R. Collins, Appl. Phys. Lett. 24, 565 (1974).

35. Fred A. Sachs and Philip E. Howard, Electro-Optical Systems Design, October, 1975, p. 34.

36. H. A. Lewis and M. B. Denton, J. Automatic Chem. 3, 9 (1981).

37. M. B. Denton, H. A. Lewis and G. R. Sims, "Charge-Injection and Charge-Coupled Devices in Practical Analysis: Operation Characteristics and Considerations," in Multichannel Image Detectors, Vol. 2, Yair Talmi, ed., ACS Symposium Series Vol. 236, American Chemical Society, Washington, D.C. (1983), p. 133.

38. D. F. Barbe, ed. "Charge Coupled Devices", Topics in Applied Physics, Vol. 38, Springer-Verlag, Berlin, (1980), Ch. 2, p. 9.

39. J. D. Ingle, Jr. and S. R. Crouch, Anal. Chem. 43, 1331 (1971).

40. H. Mishima, Opt. Commun. 4, 434 (1971).

41. Hamamatsu Photomultiplier Tube Data Sheet.

42. J. W. Lunden, G. J. Michon and J. Carbone, 12th International Television Symposium and Thechnical Exhibition Symposium Record Equipment Inovations Sessions, Montreux (1981).

43. G. R. Sims and M. B. Denton, manuscript in preparation.

44. L. Mortara and A. Fowler, SPIE Proceedings 290, 28 (1981).

Table One

CPU	OB68K	MC68000 based microcomputer Omnibyte Corporation, West Chicago, IL
Chassis	System 80	Multibus standard Intel Corporation, Aloha, OR
Memory	MM-8086D	0.5 Mbyte dynamic RAM (2) Micro Memory Inc., Chatsworth, CA
Mass Storage	MRX 450	5 Mbyte fixed, 5 Mbyte removable Memorex Corporation, Santa Clara, CA
Host Adapter	DTC-86	Data Technology Corporation, Santa Clara, CA
Terminal	Z29	Zenith Data Systems, Saint Joseph, MI
Printer	DP9501	Anadex Corporation, Chatsworth, CA
Software	IOForth	IO Incorporated, Tucson, AZ

FIGURE CAPTIONS

Figure 1a,b

a. Schematic representation of a linear photodiode array. Each diode and its associated capacitance is successively connected to the video line by action of the shift register. Diode capacitances are recharged by turning on the reset transistor.
b. Schematic representation of a single photodiode element showing diode capacitance and video line capacitance. Once the diode capacitance is recharged, the select switch is opened leaving an uncertainty in the voltage on the diode capacitance, the magnitude of which is given by Equation 2.

Figure 2a,b,c

a. Schematic cross-section of a single CID element showing potential wells created by the application of biases to the row and column electrodes. The potential of the floated row electrode is sampled both before and after the photogenerated charge is shifted under it. Sampling after the electrode is floated and before the charge is sloshed allows measurement of the exact electrode potential and hence removal of KTC noise.
b. Electrical equivalent of a single CID element showing the connection of the video preamplifier to the row electrode throughout the reset/read process.
c. Schematic of a complete CID sensor. The vertical scanner sequentially connects rows to the video line. The horizontal scanner passes the drive signal to a selected column thus allowing the measurement of the charge information stored at the intersection of the selected row and column.

Figure 3

Signal-to-noise comparison of a solid state imager and a PMT. Signal-to-noise ratio is plotted versus integration time assuming a 5 photon per second flux.

wavelength	= 450 nm
photocathode QE @ 450 nm	= 25% (41)
imager QE @ 450 nm	= 45%
photocathode dark current	= 20 counts/second
imager read noise	= 60 carriers rms
time to measure photocathode dark current	= 60 seconds

Notice that the crossover occurs after 55 seconds at a signal-to-noise ratio of 2.

Figure 4a,b

a. The topology of the CID-17 sensor. No structures between detector elements results in good spectral responsivity.
b. Cross-section of of a single CID-17 detector element. Charge is shown stored under the column electrode. Charge is sensed by sloshing the charge under the split row electrode.

Figure 5

The CID-17 camera head mounted on the test apparatus used for measurement of various electro-optical properties. The aperture stops allow illumination of only the central portion of the sensor.

Figure Captions Cont.

Figure 6
Apparatus used for quantum efficiency measurements.

Figure 7a,b
Effect of re-reads on the measured signal level. a. Shown as a percentage of full scale. b. Shown on a greatly expanded scale.

Figure 8
Reduction of the system read noise by performing successive non-destructive re-reads. 400 re-reads reduces system read noise from 960 charge carriers to 58 charge carriers.

Figure 9a,b
Response of the CID-17 to light. a. Signal versus light level. b. First derivative of signal-versus-light level showing first order curvature in response.

Figure 10a,b
Linearized counterparts of Figure 9.

Figure 11
Demonstration of the efficiency of the charge removal procedure. One 10 microsecond inject cycle efficiently removes all photogenerated charge from the array regardless of initial signal level.

Figure 12
The mean-variance method of system gain determination involves measurement of variance due to photon shot noise and mean signal level at a number of exposure levels. A plot of the data results in a line with slope equal to the inverse of the system gain. In this case, 30 charge carriers per analog to digital converter unit.

Figure 13
Schematic of the CID-17 showing the de-select register which maintains the potential of each row not conected to the video line by the vertical scanner.

Figure 14
Schematic of a CID sensor showing the capacitive coupling which exists between row and column electrodes. When charge is sloshed along a column, a change in the potential along the unselected rows is induced. This potential change is then coupled into the selected row, appearing as video signal.

Figure 15
Illustration of the CID array showing the regions used for the study of crosstalk. A circular region near the center of the device was illuminated by the LED in the test apparatus. An entire column passing through the illuminated region was read in order to measure the total photogenerated charge collected by that column. A subarray in the unexposed region was used to measure the extent of the crosstalk.

Figure Captions Cont.

Figure 16
A plot of the crosstalk measured along a column as a function of the total integrated charge along that column. The crosstalk is seen to be proportional to the total integrated charge and on the order of 0.07 percent.

Figure 17
Quantum efficiency comparison for the CID-17BAS and two opaque photocathode materials.

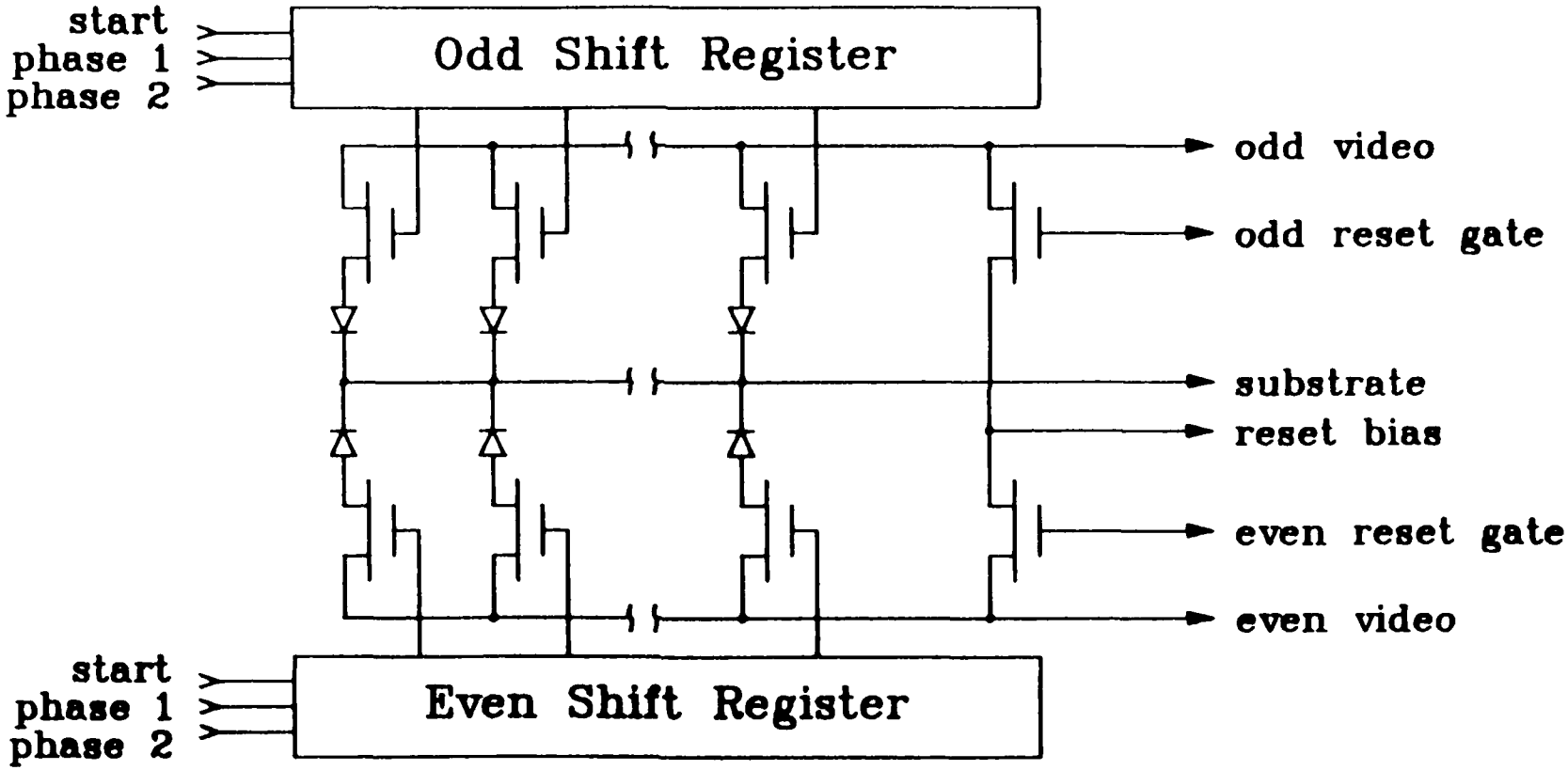
start
phase 1
phase 2
Odd Shift Register
odd video
odd reset gate
substrate
reset bias
even reset gate
even video
start
phase 1
phase 2
Even Shift Register

FIGURE 1a

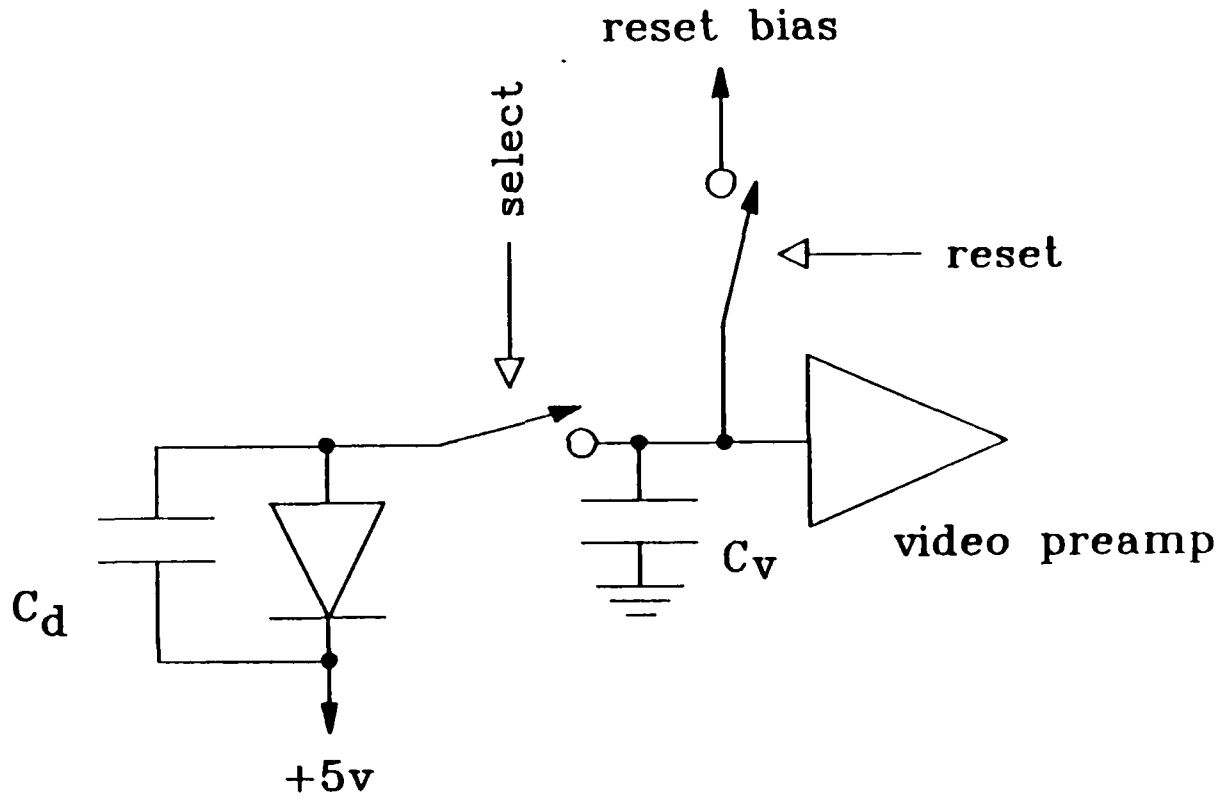

FIGURE 1b

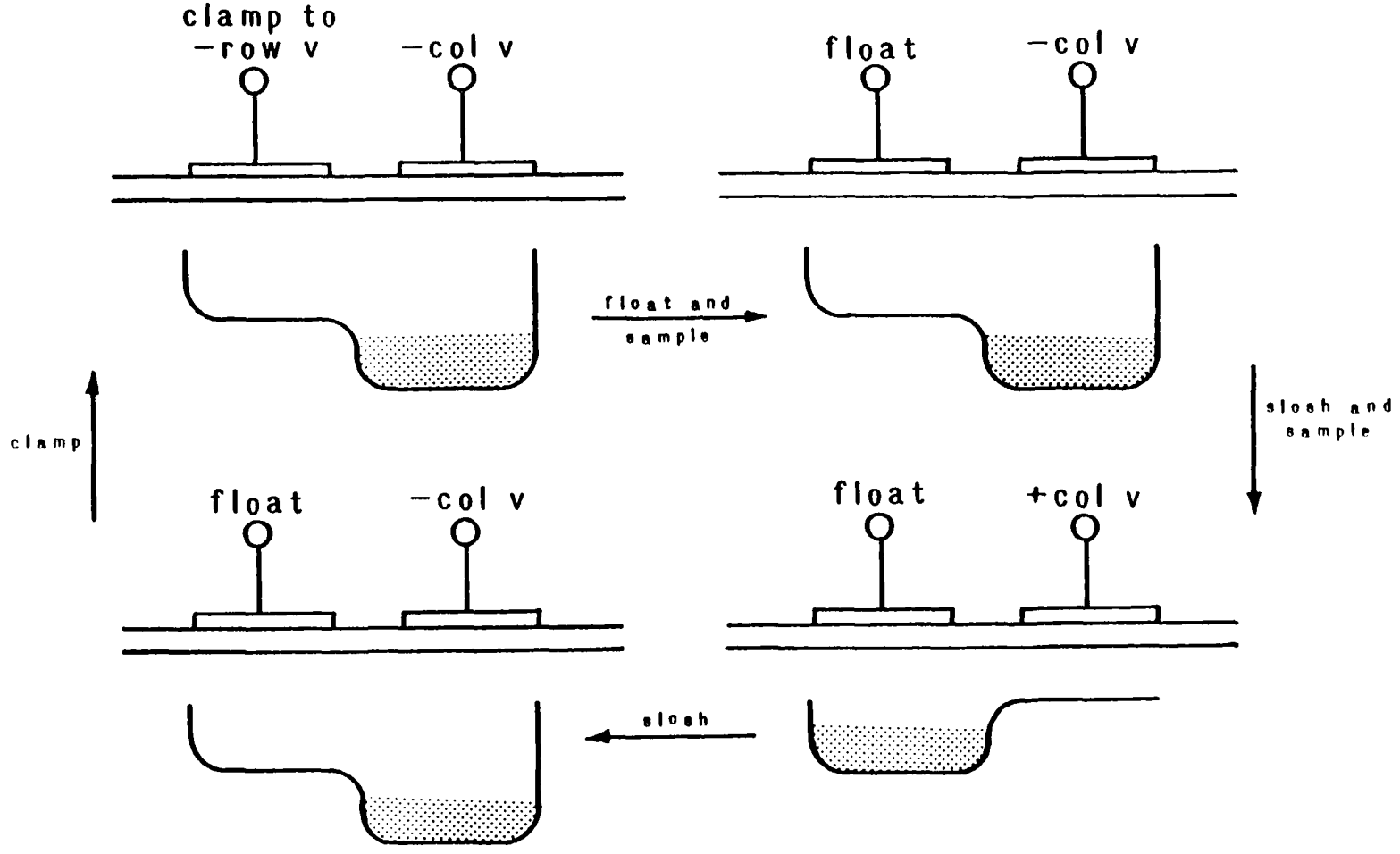
clamp to
−row v
−col v
float
−col v
float and
sample
clamp
slosh and
sample
float
−col v
float
+col v
slosh

FIGURE 2a

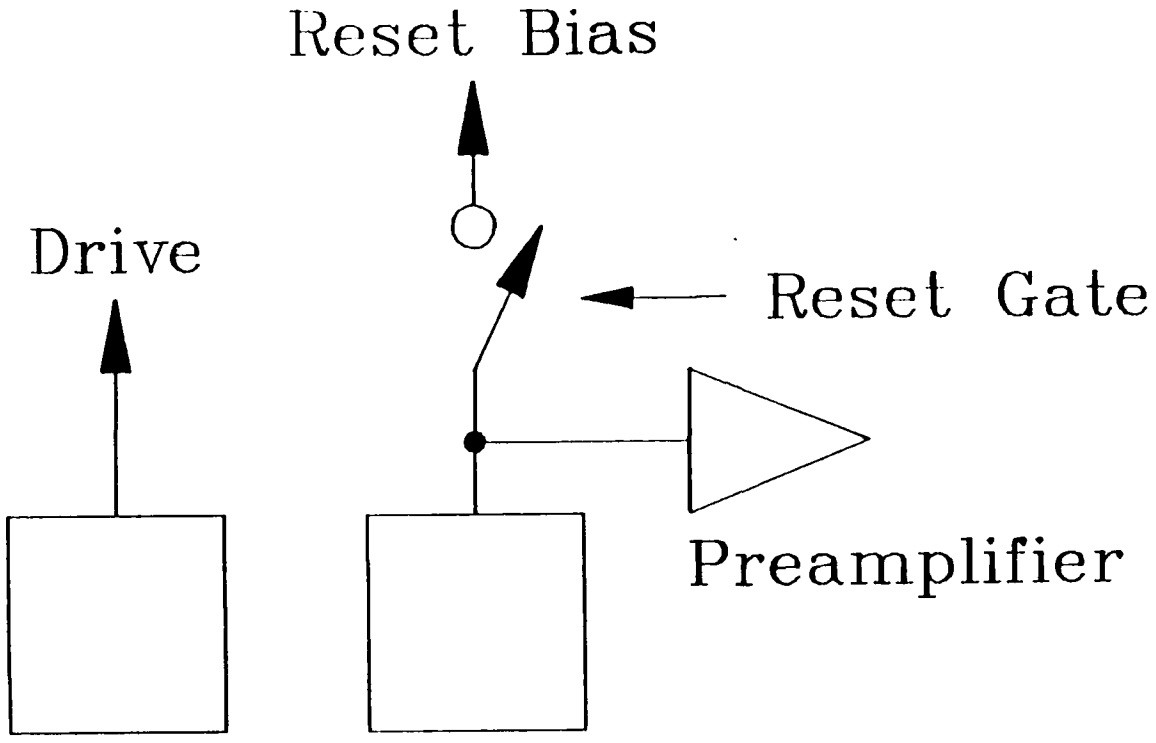

FIGURE 2b

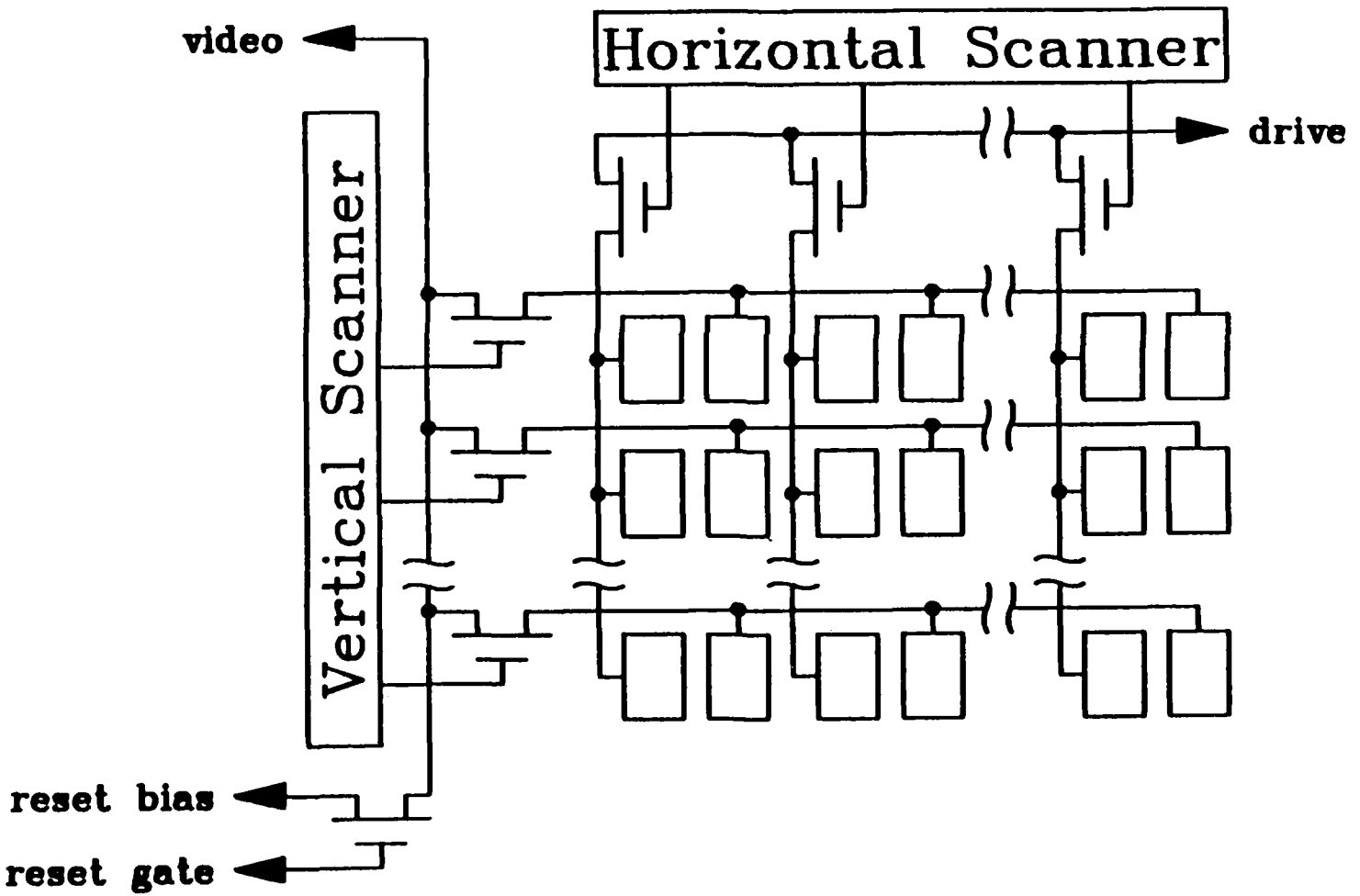
video
Horizontal Scanner
drive
Vertical Scanner
reset bias
reset gate

FIGURE 2c

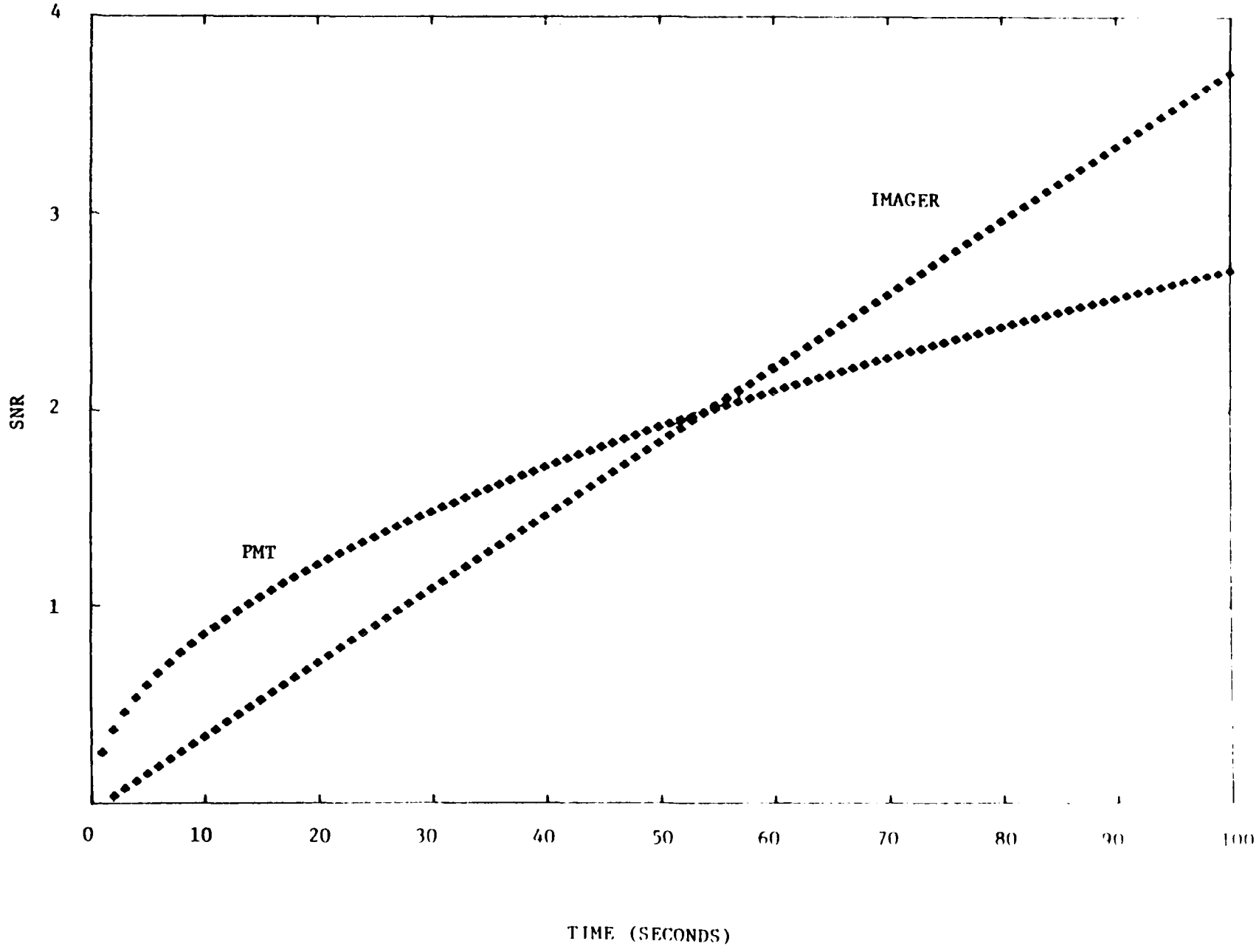
4
3
2
1
SNR
IMAGER
PMT
0
10
20
30
40
50
60
70
80
90
100
TIME (SECONDS)

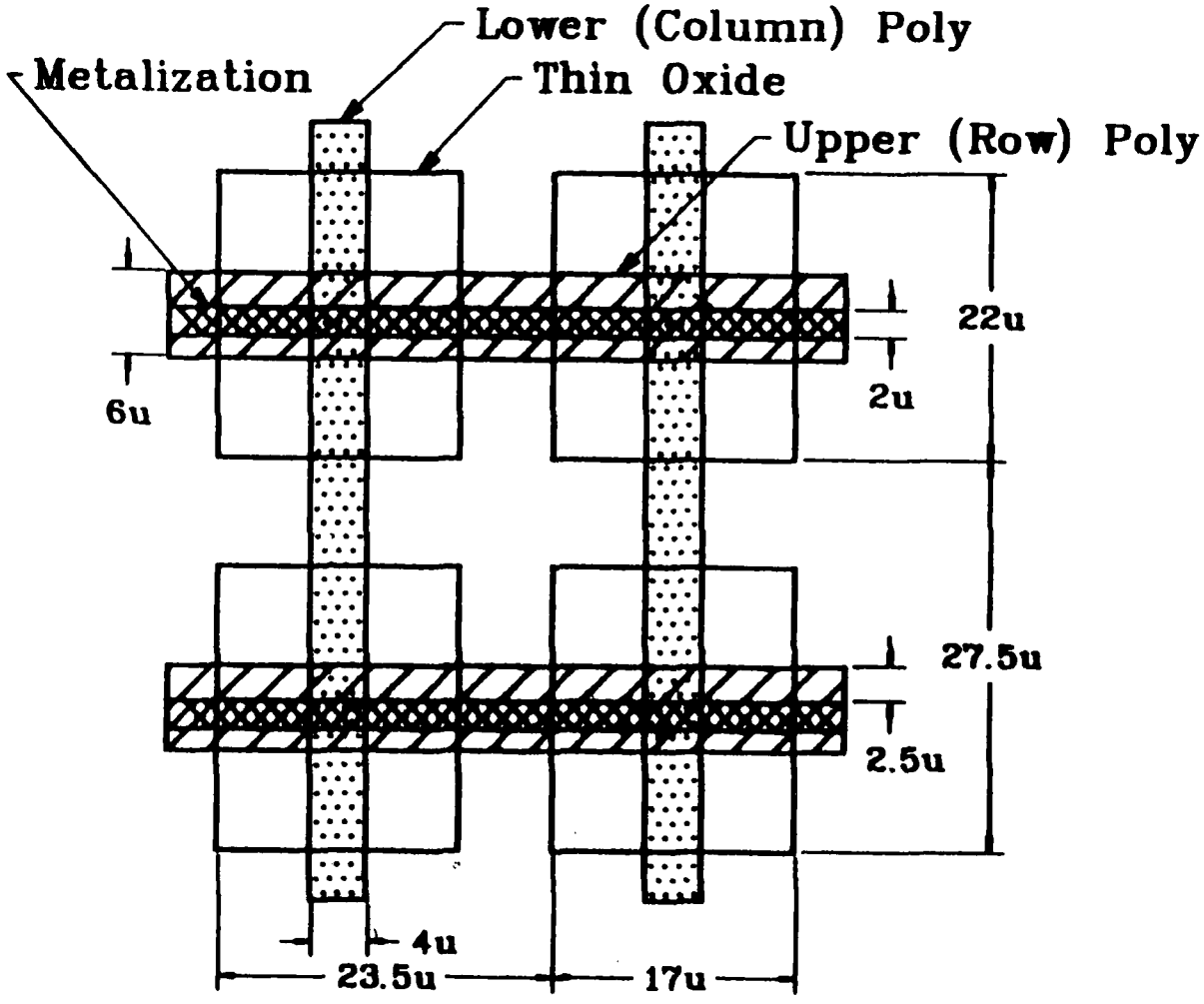
Lower (Column) Poly
Metalization
Thin Oxide
Upper (Row) Poly
22u
2u
6u
27.5u
2.5u
4u
23.5u
17u

FIGURE 4a

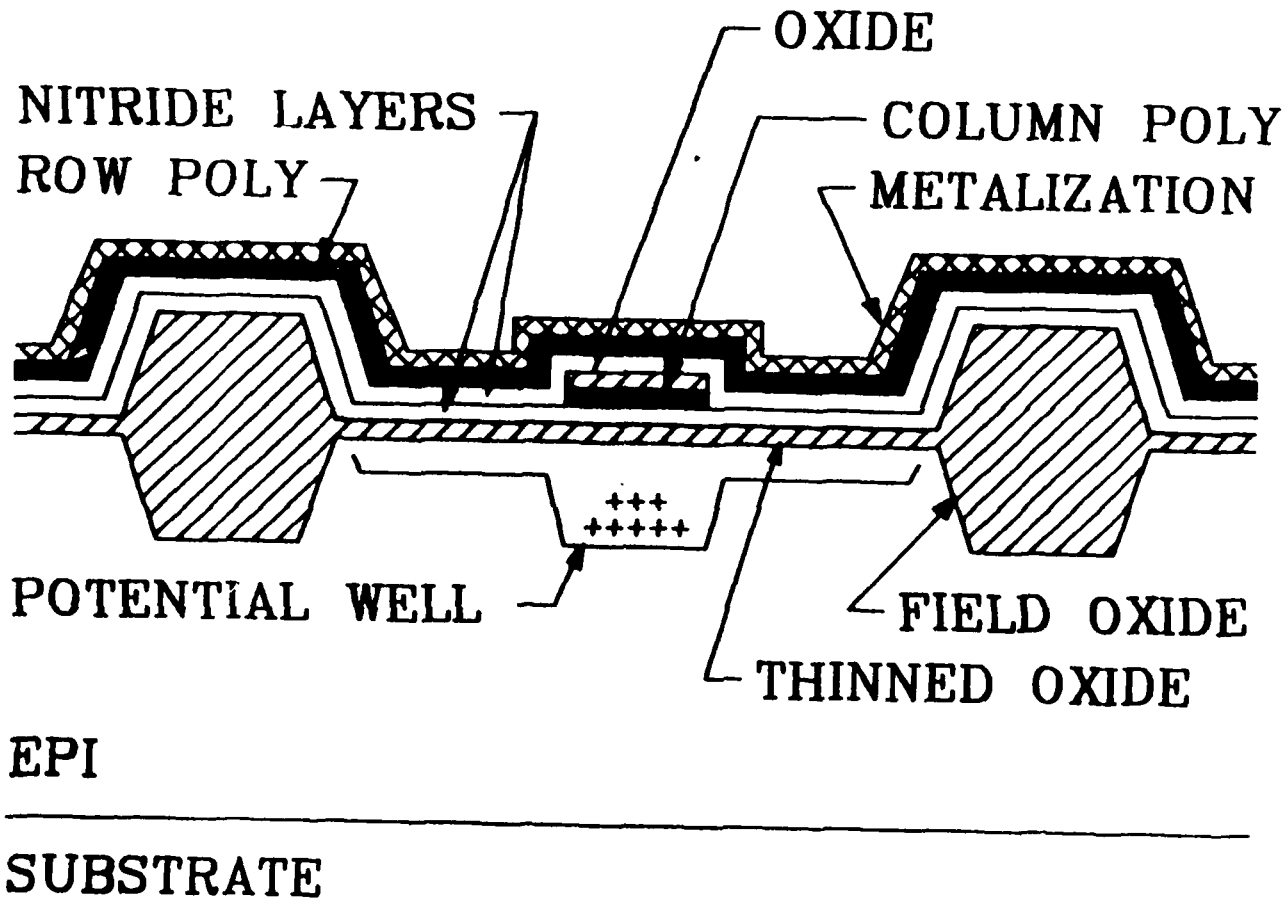
OXIDE
NITRIDE LAYERS
COLUMN POLY
ROW POLY
METALIZATION
+++
++++
POTENTIAL WELL
FIELD OXIDE
THINNED OXIDE
EPI
SUBSTRATE

FIGURE 4b

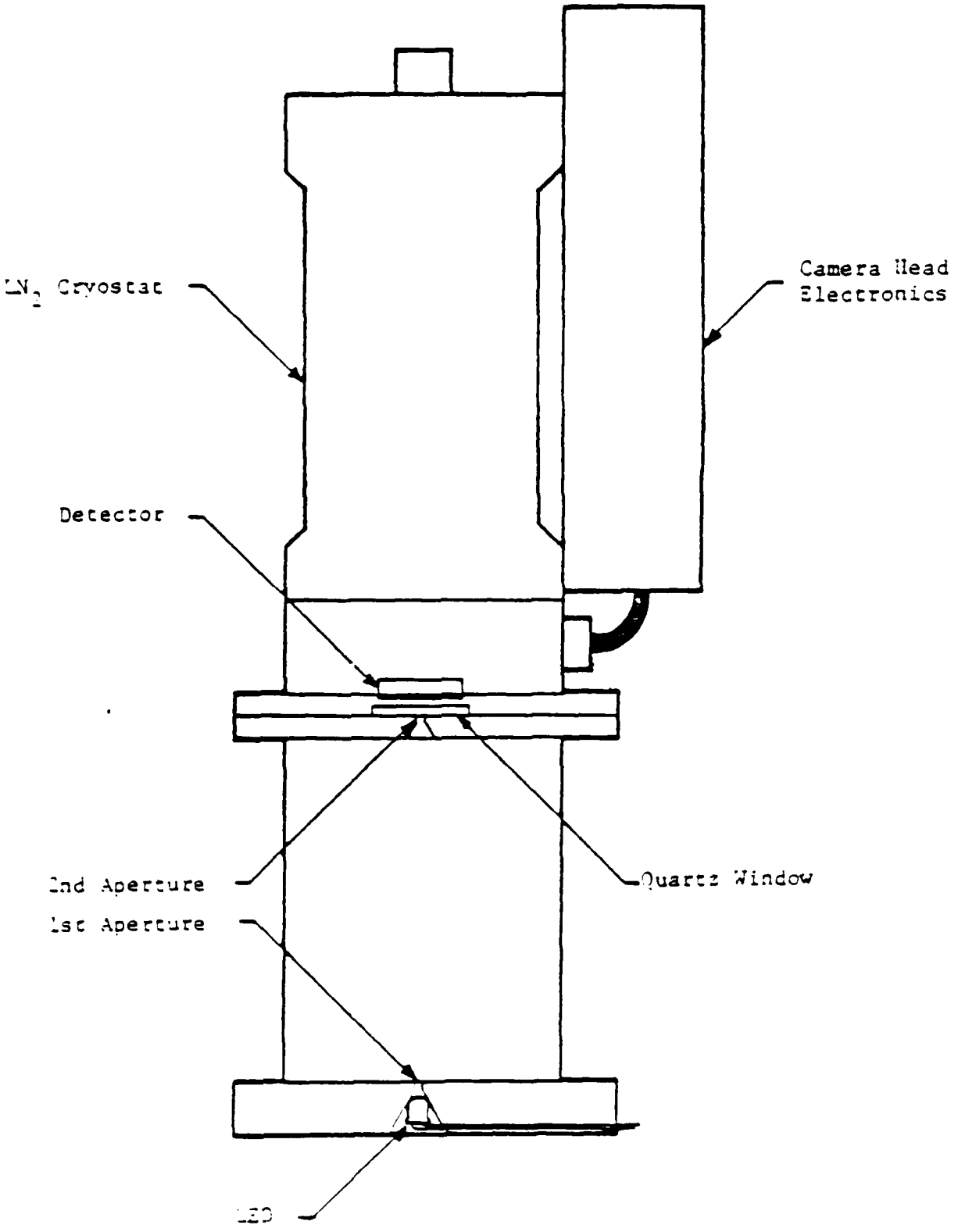

GENERAL PURPOSE TEST APPARATUS

FIGURE 5

QUANTUM EFFICIENCY APPARATUS

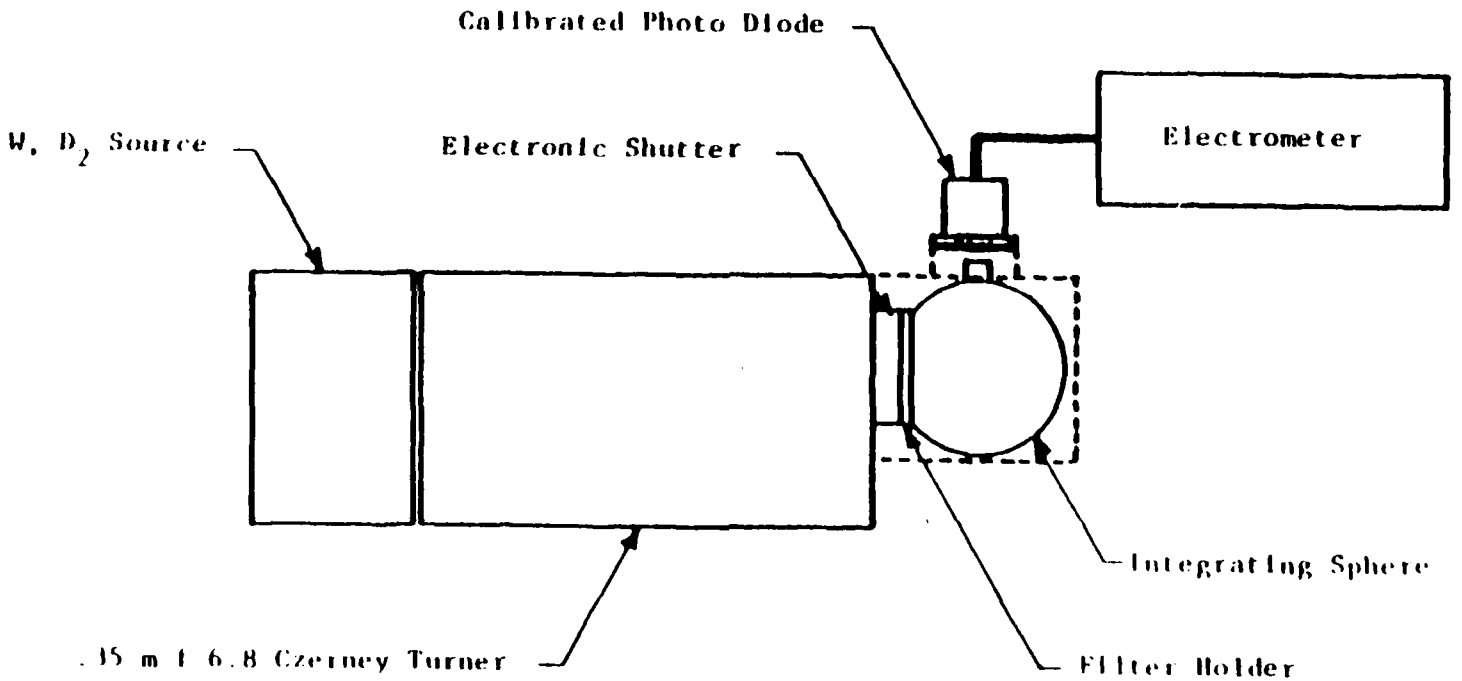

FIGURE 6

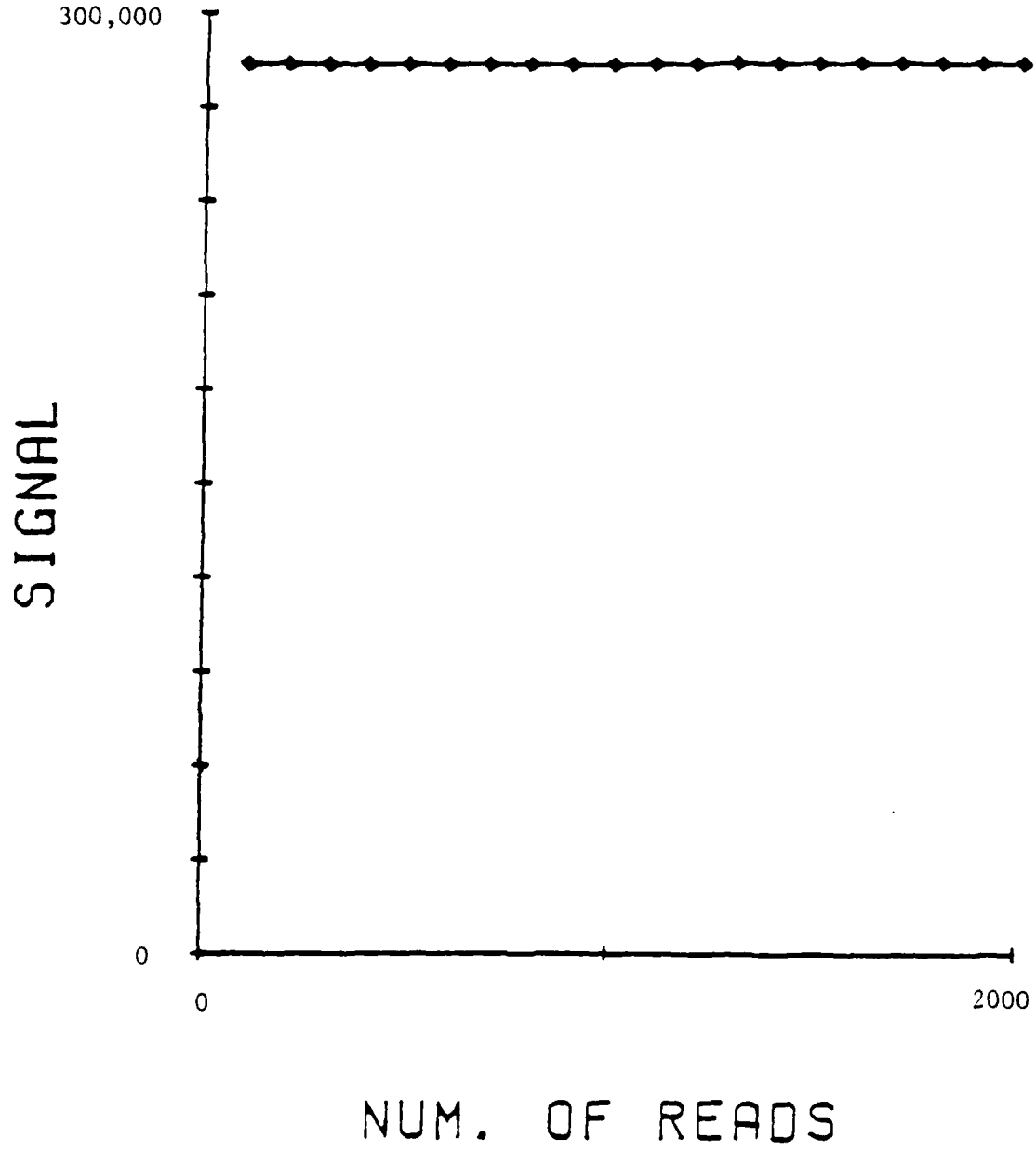

Effect of Re-Reads

FIGURE 7a

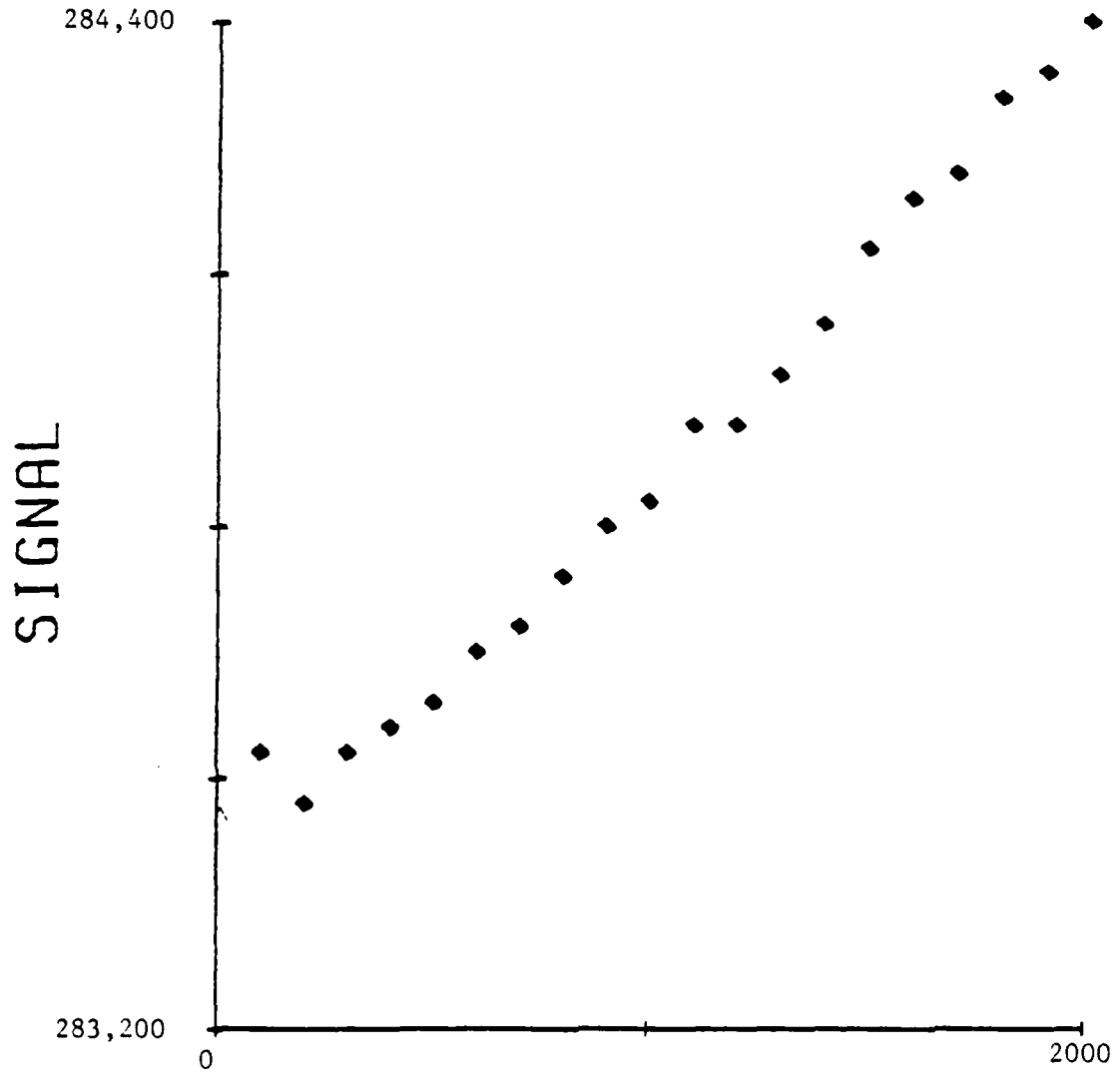

EFFECT OF RE-READS

FIGURE 7b

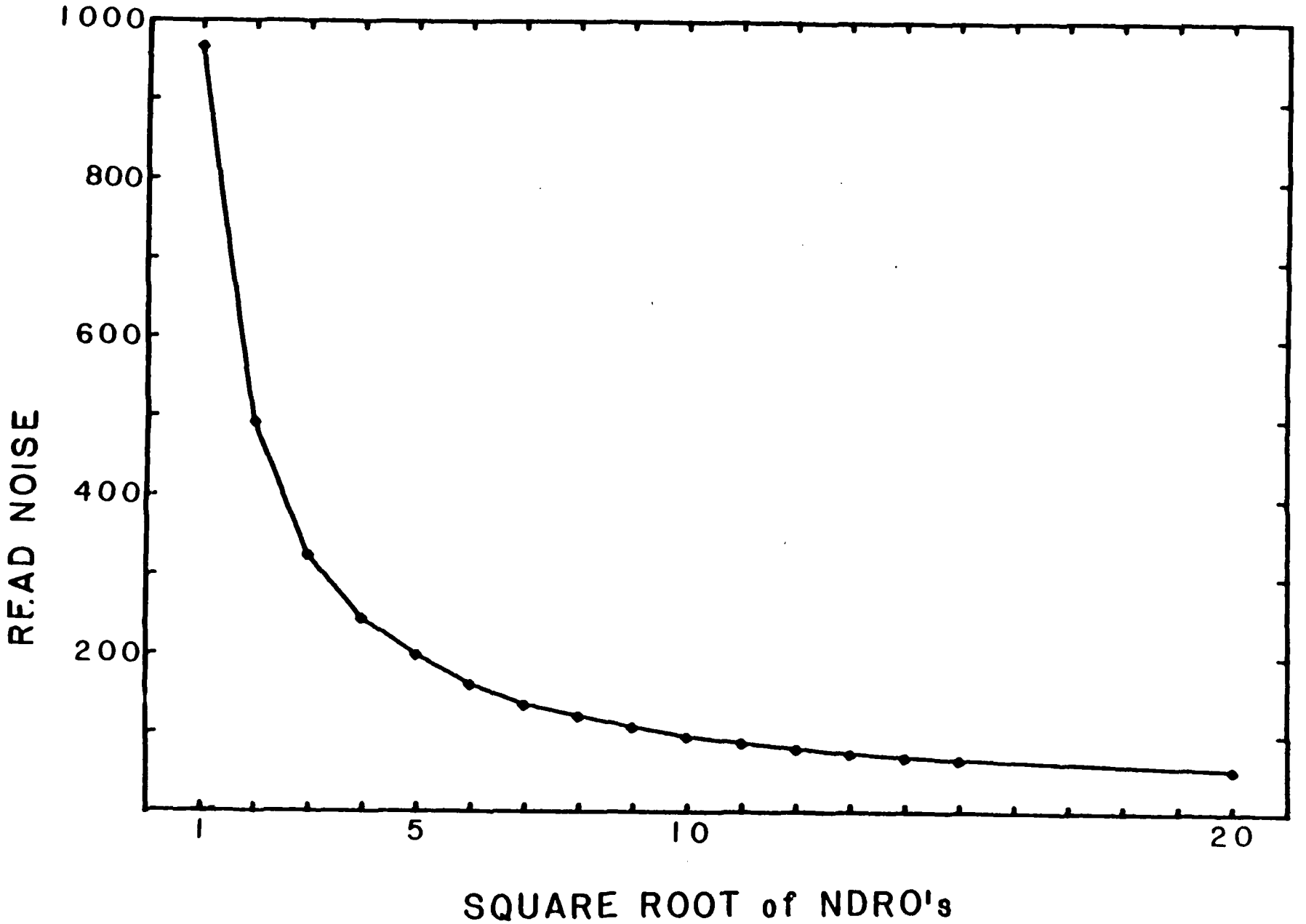
READ NOISE vs NDRO's for CID-17BAS SYSTEM
1000
800
600
400
200
READ NOISE
1
5
10
20
SQUARE ROOT of NDRO's

FIGURE 8

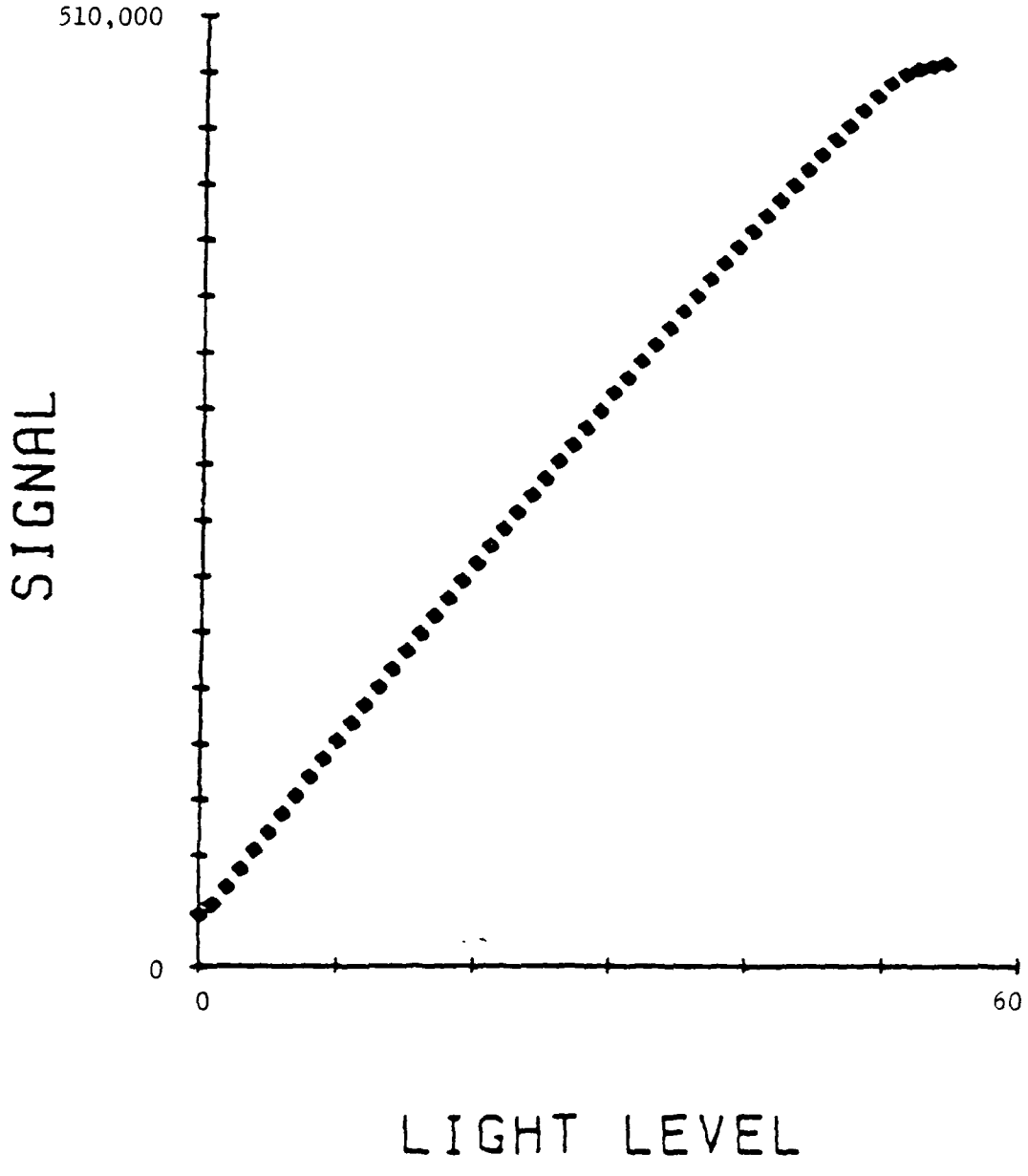

LINEARITY

FIGURE 9a

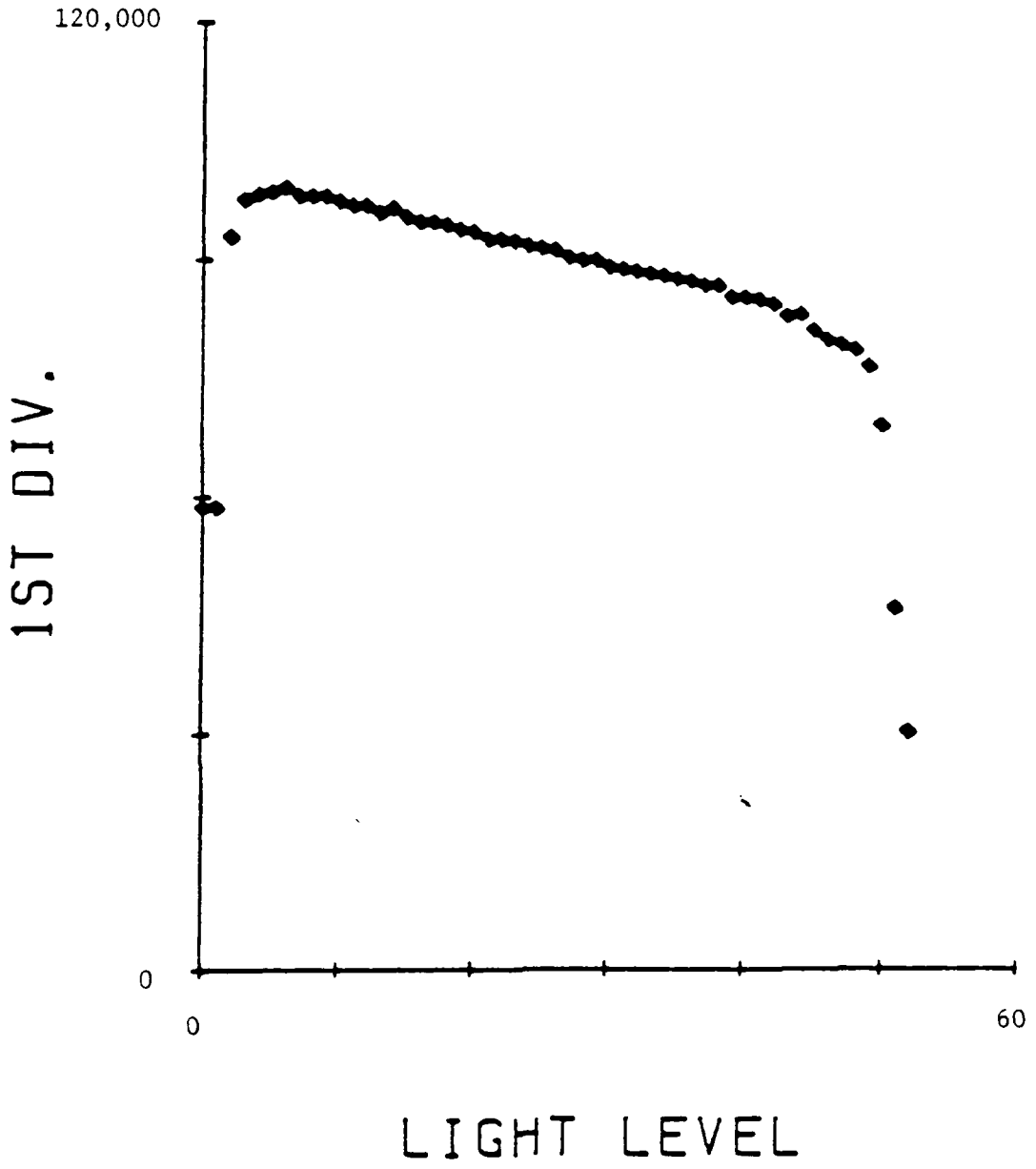

LINEARITY

FIGURE 9b

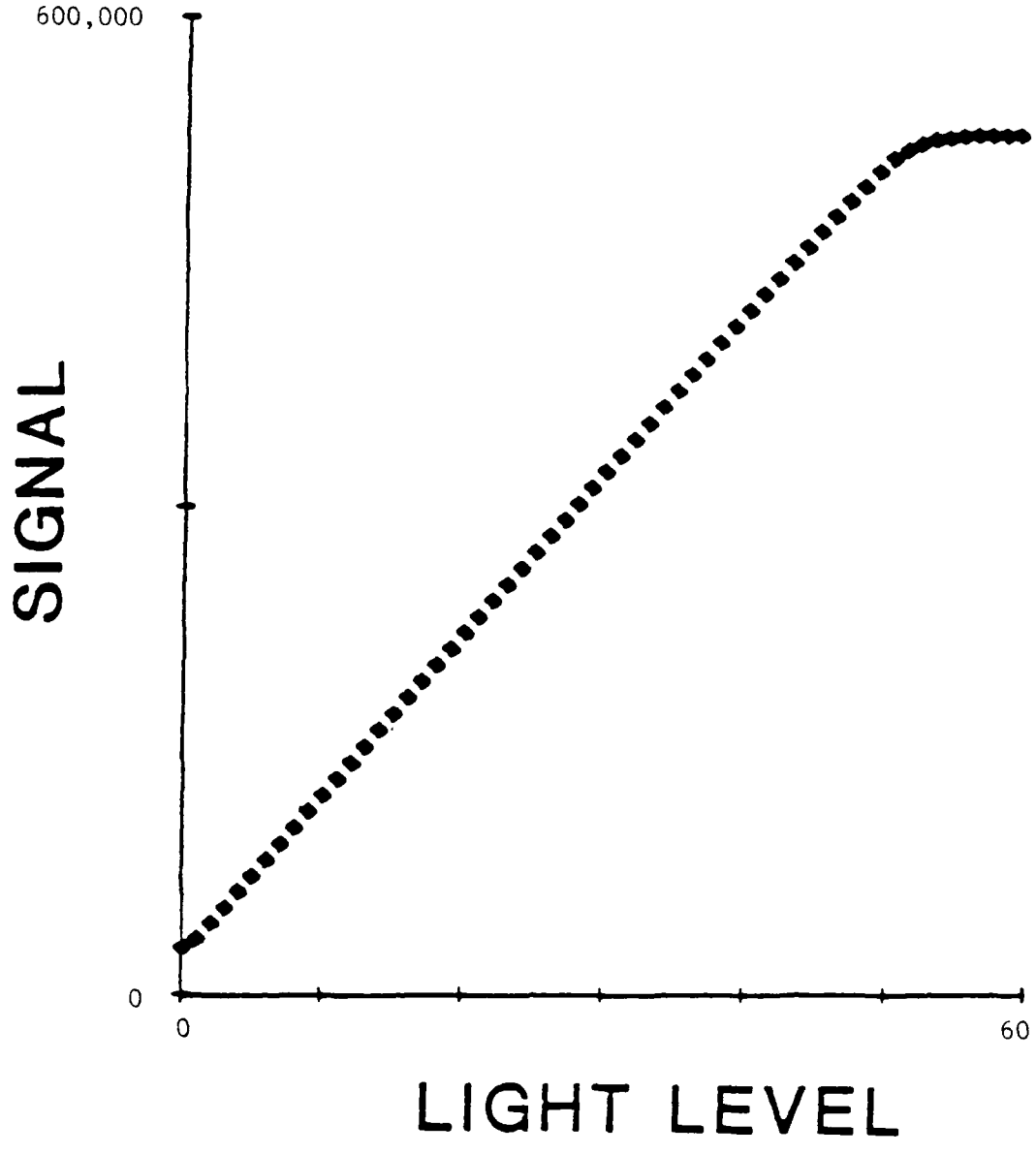

LINEARITY

FIGURE 10a

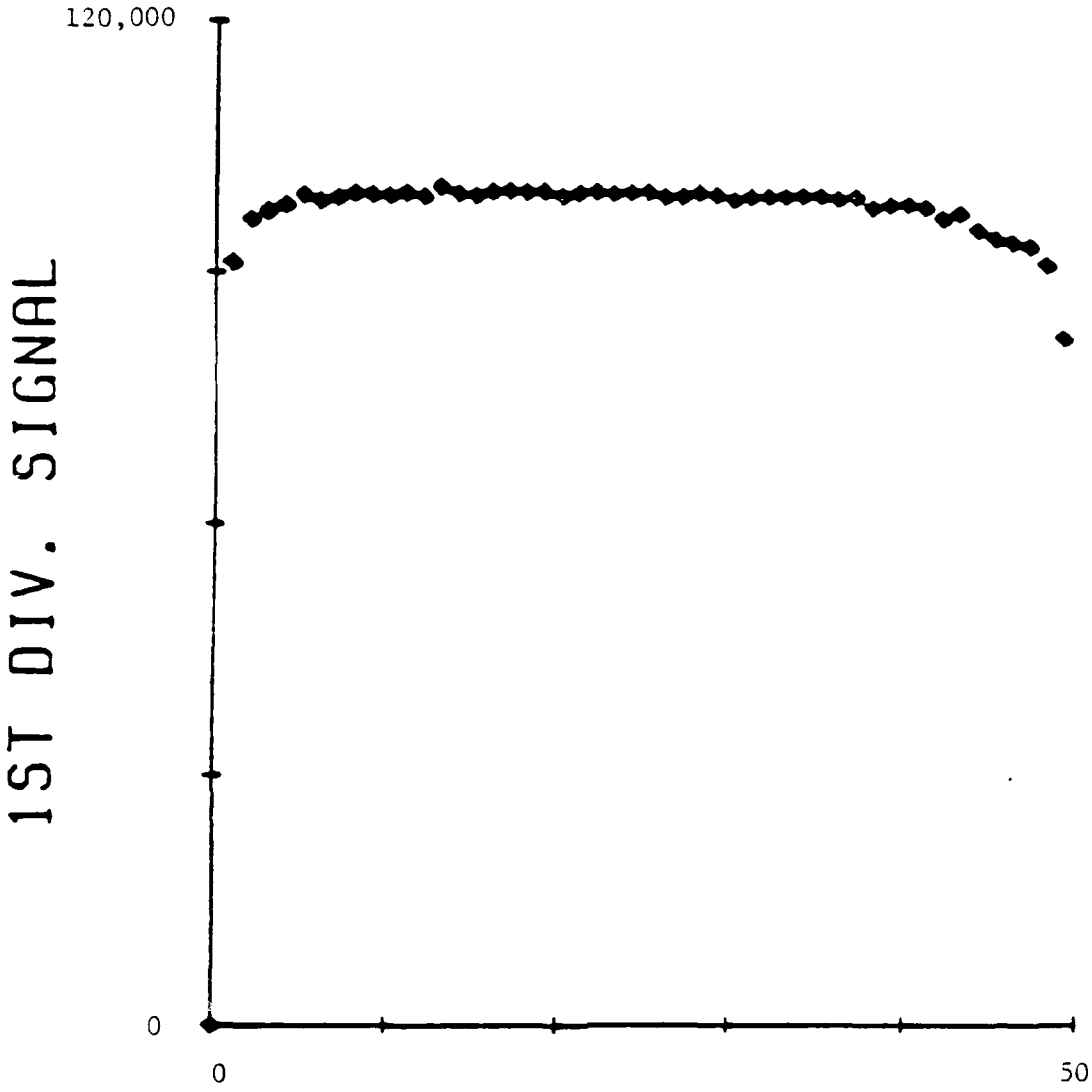

LINEARITY

FIGURE 10b

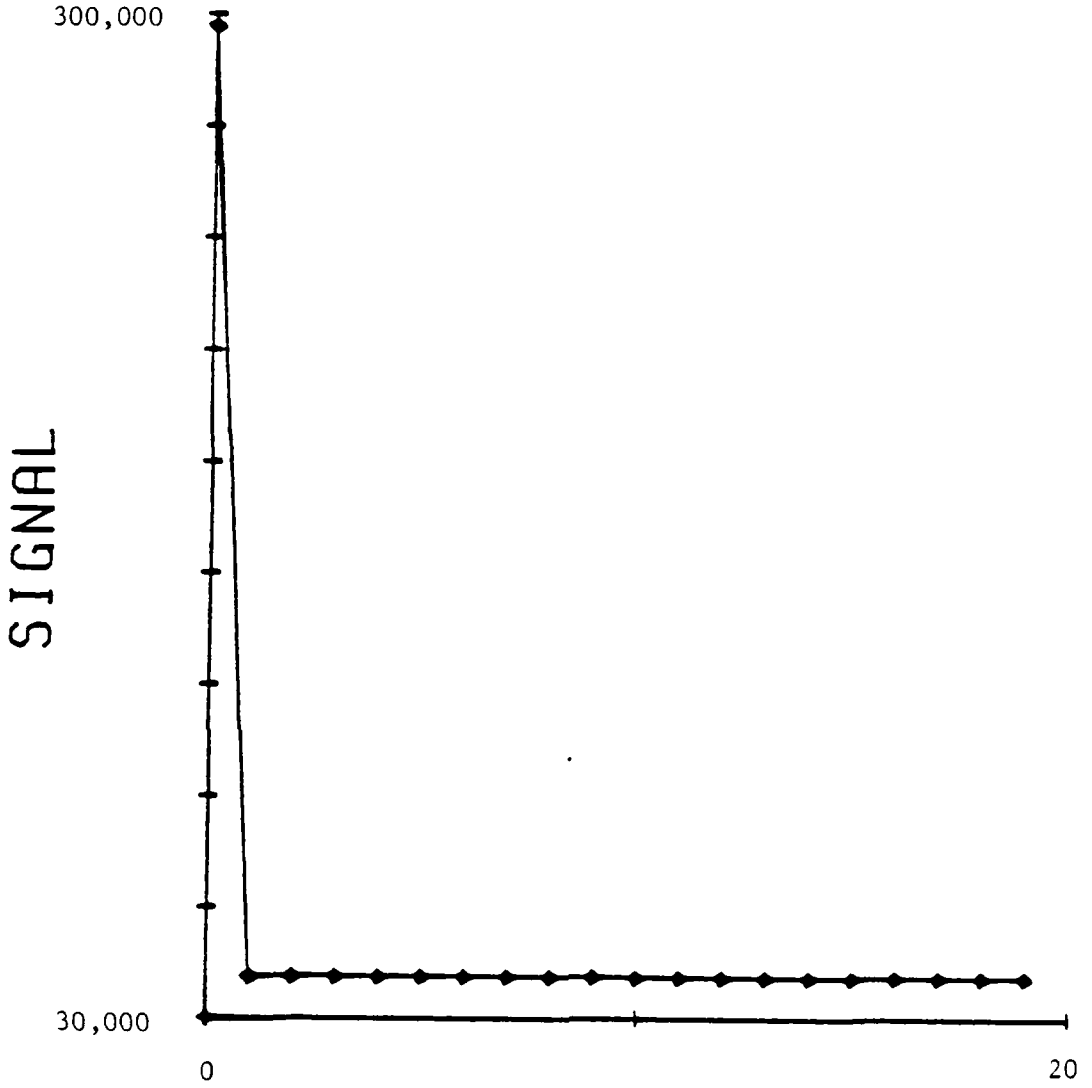

THOROUGHNESS OF INJECT

FIGURE 11

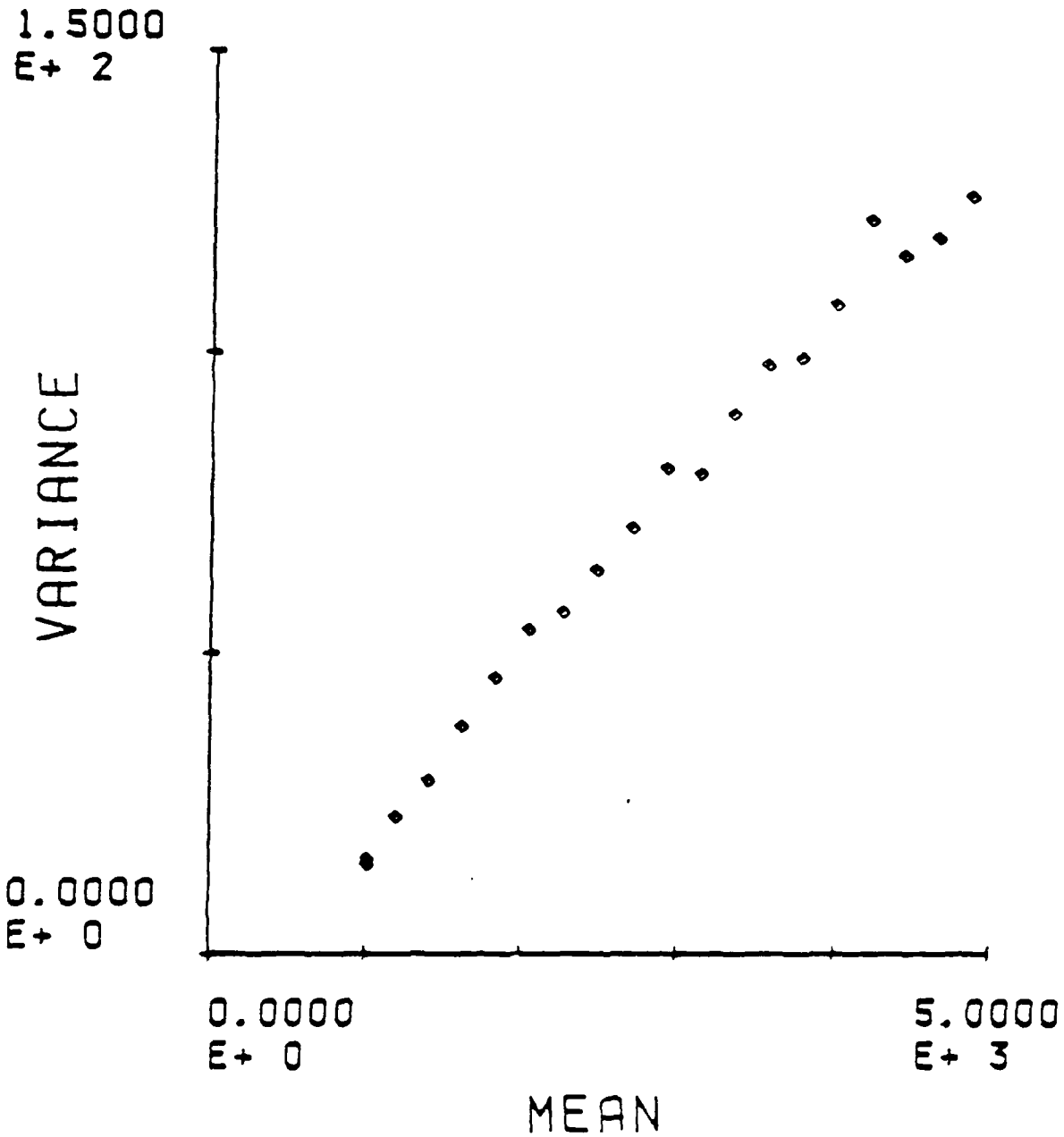

FIGURE 12

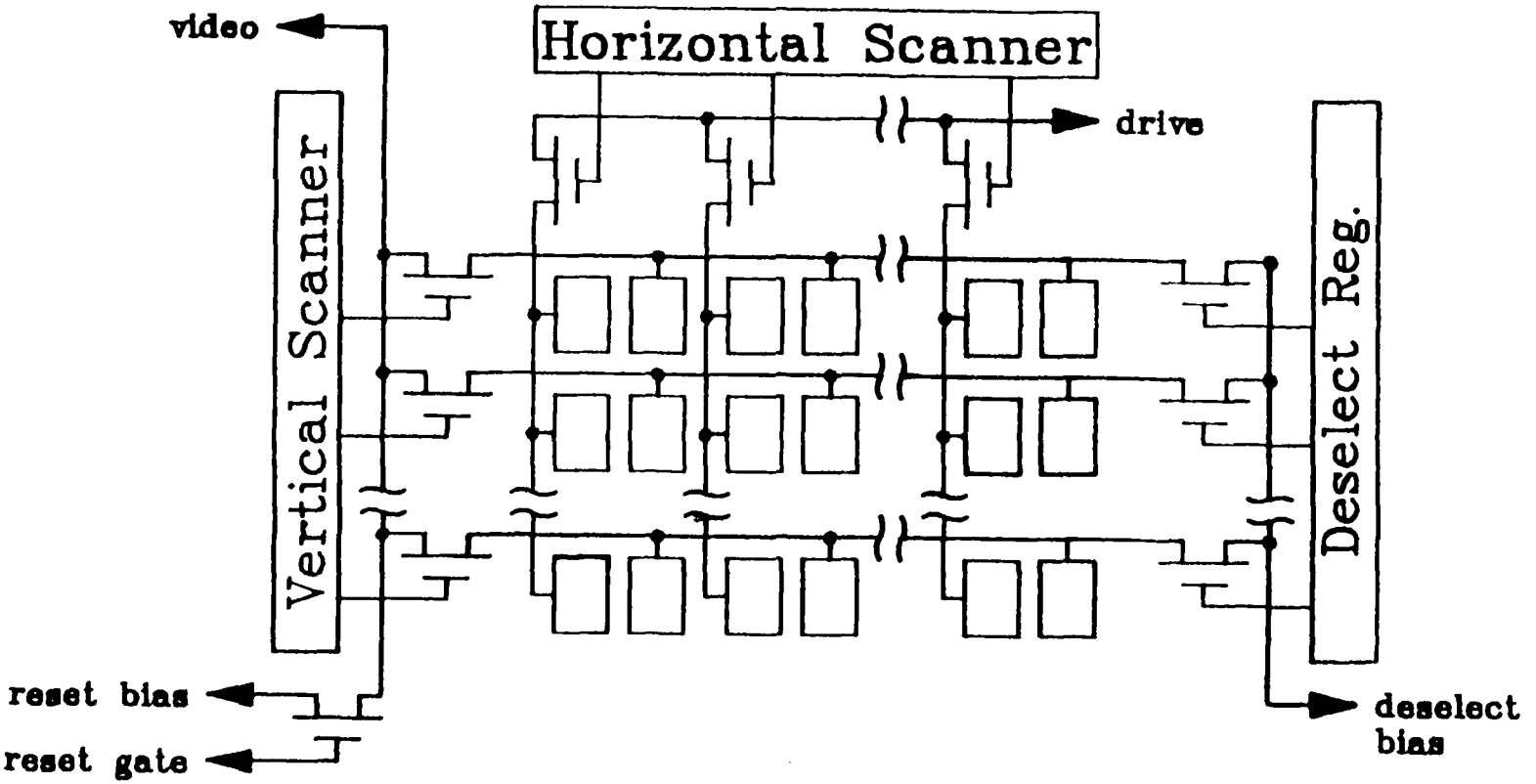
video
Horizontal Scanner
drive
Vertical Scanner
Deselect Reg.
reset bias
reset gate
deselect
bias

FIGURE 1

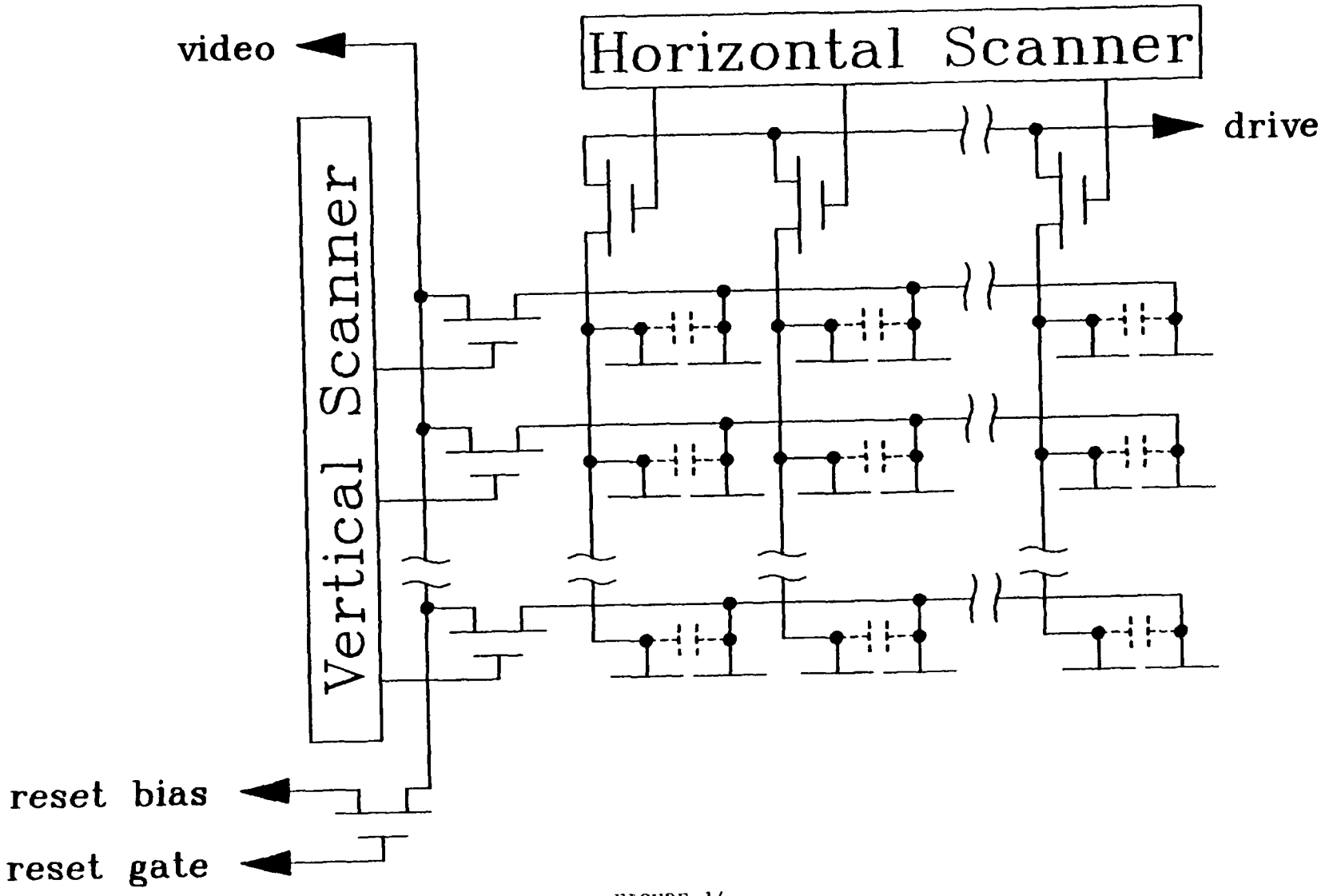
video
Horizontal Scanner
drive
Vertical Scanner
reset bias
reset gate

FIGURE 14

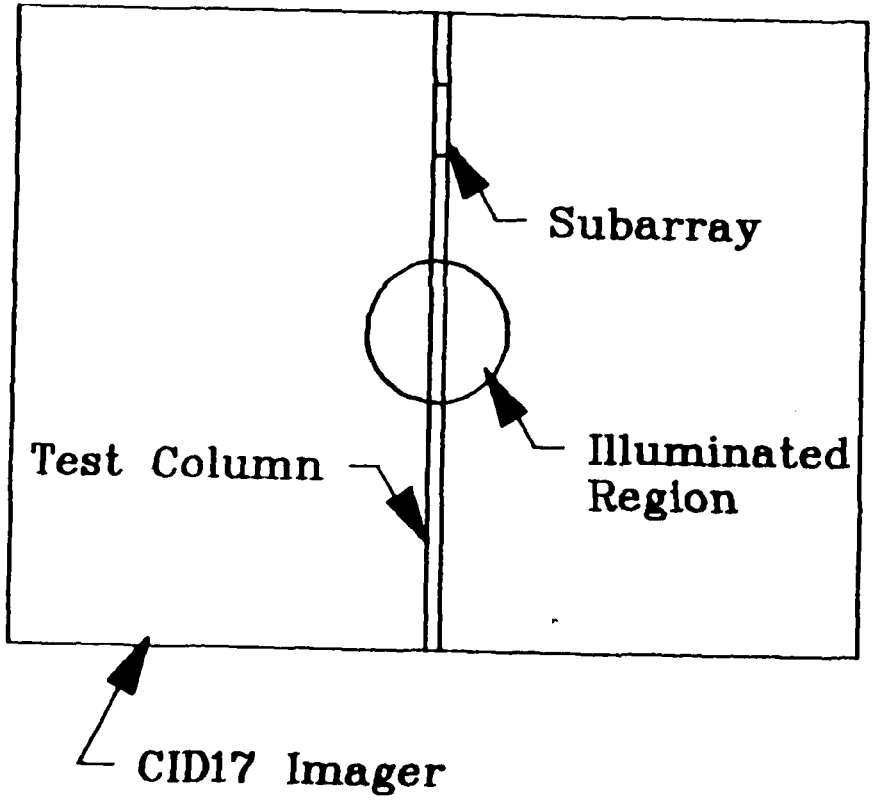

FIGURE 15

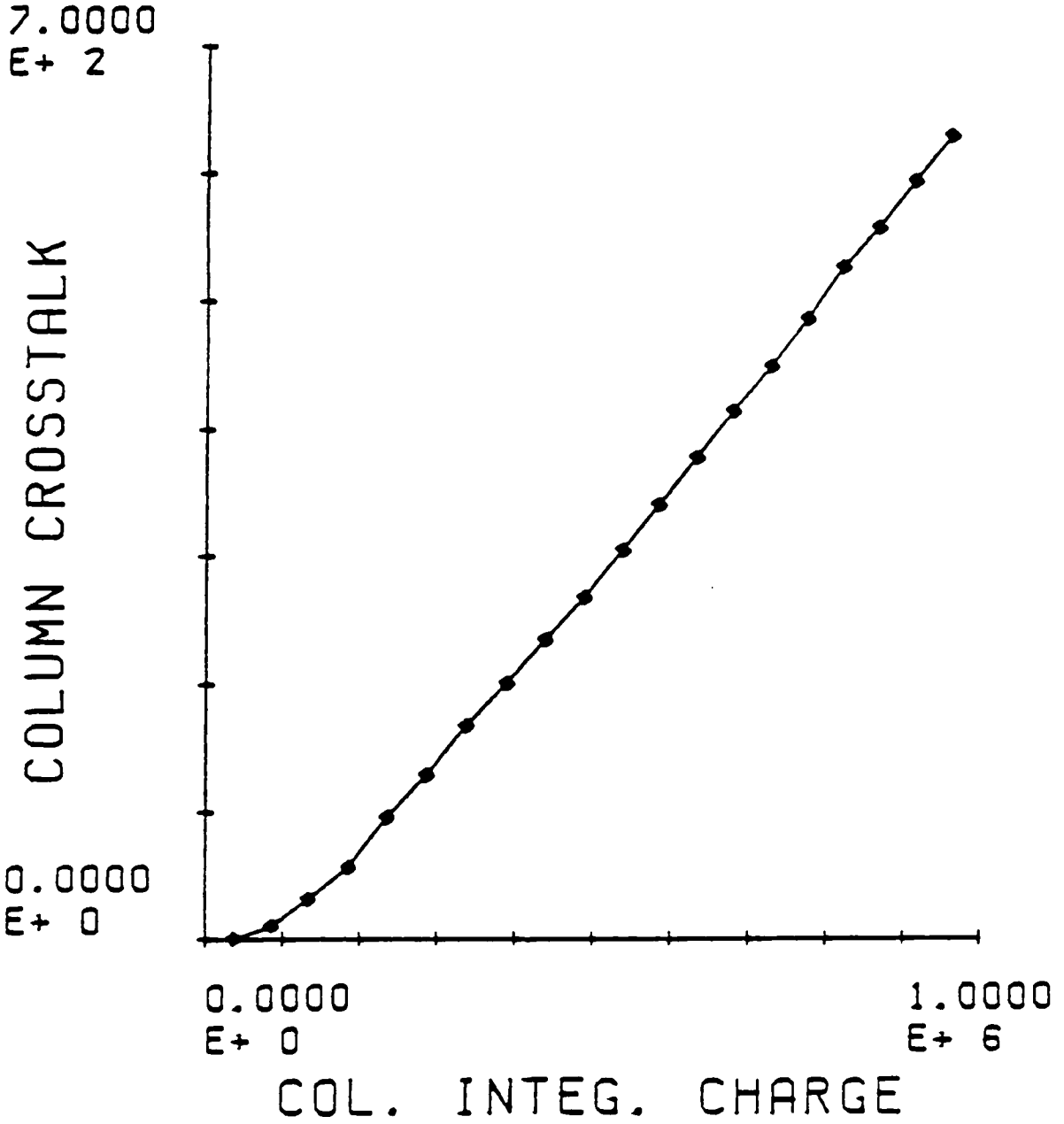

CROSSTALK

FIGURE 16

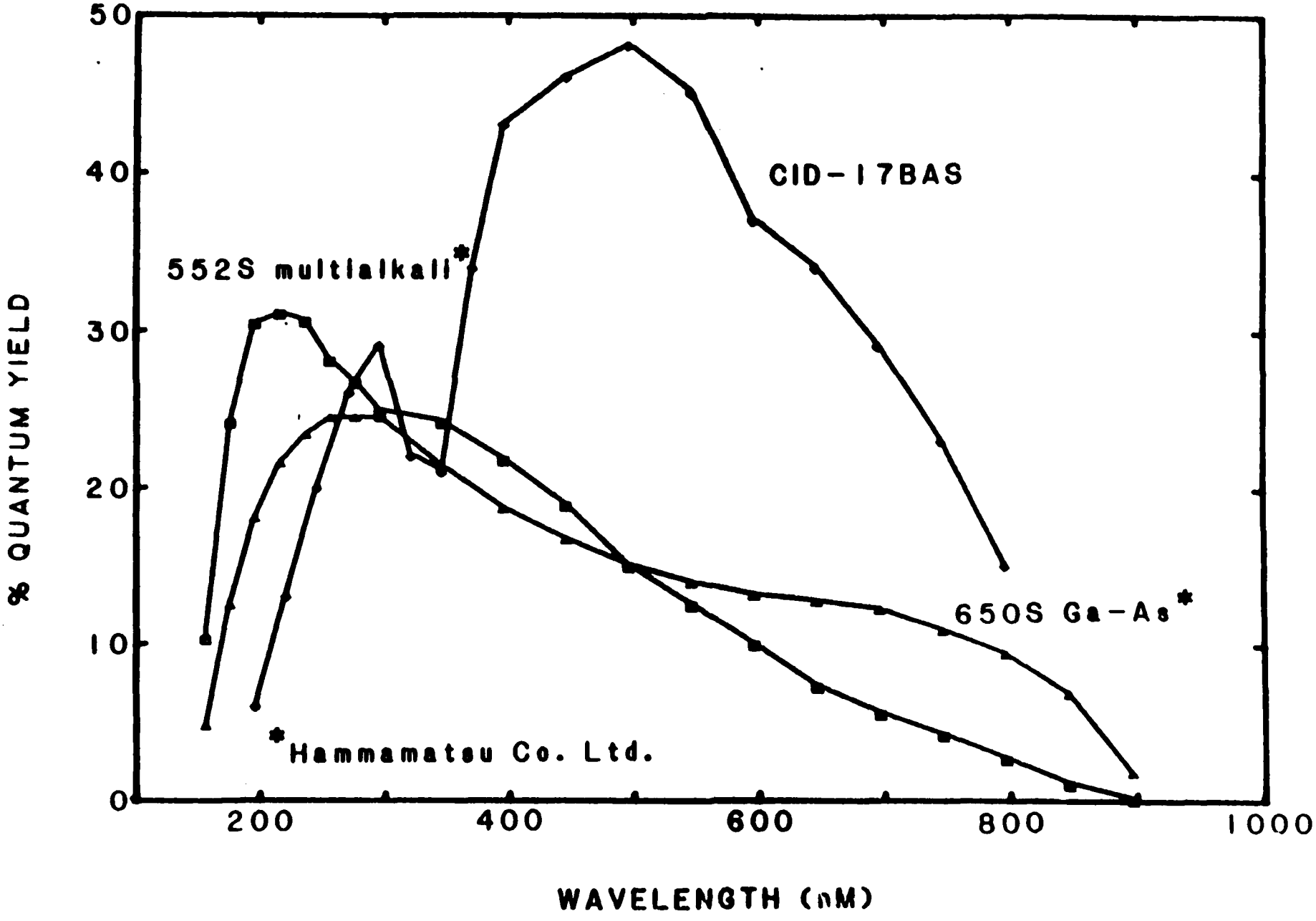
QUANTUM YIELD of the CID-17BAS vs
TWO OPAQUE PHOTOCATHODES
50
40
30
20
10
0
% QUANTUM YIELD
552S multialkali*
CID-17BAS
650S Ga-As*
*Hammamatsu Co. Ltd.
200
400
600
800
1000
WAVELENGTH (nM)

FIGURE 17

END

FILMED

2-86

DTIC